Tunable topological interface states in one-dimensional inerter-based locally resonant lattices with damping

Milan Cajić[a,b,*], Danilo Karličić[b], Johan Christensen[c], Sondipon Adhikari[d]

[a]*Faculty of Science and Engineering, Swansea University, Swansea SA1 8EN, UK*
[b]*Mathematical Institute SANU, 11000 Belgrade, Serbia*
[c]*Department of Physics, Universidad Carlos III de Madrid, ES-28916 Leganès, Madrid, Spain*
[d]*James Watt School of Engineering, The University of Glasgow, Glasgow G12 8QQ, UK*

Abstract

Wave dispersion and topology of phononic crystals in classical mechanical systems are well understood and extensively studied subjects. However, the topological properties of acoustic metamaterials with more complex unit cells having several masses, internal resonators, and inerter elements is an insufficiently investigated topic. In this work, we study a class of locally resonant acoustic systems having diatomic- and triatomic-like mass-in-mass unit cells with inerter elements and different springs connecting outer masses. Winding numbers and signs of band gaps are investigated to assess the topological characteristics of a lattice band structure that support edge/interface modes and whether that property is affected when inerter elements are embedded into the system. The dynamics of finite undamped and damped chains constituted of two connected sub-lattices are investigated to demonstrate the existence of interface modes and their localization in space. We reveal that the presented diatomic-like and triatomic-like mass-in-mass chains can generate several interface modes that reside within both lower and higher frequency band gaps. The concept is illustrated through the investigation of the eigenvalue spectrum for varying and fixed stiffness of outer springs and frequency response function. The effect of arbitrary viscous damping is explored based on steady-state responses of the lattice interface mass points. Numerical analysis reveals that the introduction of inerters in combination with local resonators can significantly shift the band gaps and corresponding interface modes to lower frequency values while keeping the main topological properties of the initial configuration without inerters. The effect of damping is shown to be significant and capable to attenuate both lower and higher frequency interface mode amplitudes. We anticipate that this study will pave the wave for future works on the topic that include more reliable models of inerters in the topological mechanical metamaterial design.

Keywords: Inerters; Interface modes; Band inversion; Locally resonant metamaterials; Viscous damping

1. Introduction

Since the discovery of topological insulators in condensed matter physics [1] it was known that their topological properties determined by the geometrical phases are not related to the spatial scale or the physical nature of the system [2]. This initiated research on topological wave phenomena in other branches of physics such as photonics

*Corresponding author
Email address: milan.cajic@swansea.ac.uk, mcajic@mi.sanu.ac.rs (Milan Cajić)

Manuscript accepted in Journal of Sound and Vibration

[3], phononics [4], acoustics and mechanics [5–9]. If wave motion is supported by the topologically protected edge states, it can be robust to backscattering i.e. to defects and disorders in the medium. The term topology in this study refers to the topological properties of Bloch eigenmodes within the first Brillouin zone and not the geometry of the observed medium. In classical mechanical wave systems space and time properties can be easily controlled, which makes them more suitable for practical realization and detection of topological effects than in their condensed matter system counterparts [2]. Topological insulators can be considered inequivalent if they have different topologies. However, the topology can be changed at the interface of two in-equivalent insulators such that they support the topologically protected localized interface states.

Depending on how their non-trivial topology is created, one can distinguish two main groups of topological insulators in their classical mechanical setup. The first group belongs to insulators whose non-trivial topology is created by breaking the time-reversal symmetry [10–12], which is usually related to the quantum Hall effect in electronic and quantum systems. The second group refers to time-reversal-invariant systems emulating the quantum spin Hall [13] and valley Hall [14–16] effects. Such systems often use localized edge modes immune to defects and disorders for robust waveguiding of acoustic or elastic waves. Here, special attention is devoted to the band inversion effect where topological edge/interface states are generated in one-dimensional (1D) lattices. In parallel with 1D discrete mechanical phononic systems [9] this effect was also investigated in phononic-like elastic structures [17, 18]. The bulk band topological properties of such systems are usually characterized by the geometric phase, which in the 1D case is known as Zak's phase [19]. This paved the way to study topological interface states in the sub-wavelength range in translational metamaterials [20] and quasiperiodic locally resonant meta structures [21]. It was also unveiled that topological edge modes can emerge in metamaterials only from their patterning, independently from the coupling and structure of local resonators [22]. Another interesting feature of quasiperiodic acoustic lattices is that they can exhibit both, adiabatic pumping which was confirmed by mapping the edge state spectrum, and non-adiabatic pumping confirmed by mapping the Hofstadter butterfly spectrum [23].

Tuning of topological interface states can be achieved in several ways and this became an important subject of investigation among researchers. Some of the examples include a change of the shear modulus by imposing the external electric field [24] or change of contact stiffness between particles in the granular crystal [25]. Inerters are known as two-terminal devices whose terminals can move freely to provide a resisting force that is proportional to their relative acceleration due to its mass amplification effect [26–28]. In particular, these properties are often used in vibration reduction problems [29], where only by tuning the properties of the inerter device [30, 31] one can achieve optimal vibration absorption [32]. The dynamic mass-amplifying effect of inerters was applied in [33] to investigate longitudinal elastic wave propagation characteristics of acoustic metamaterials with different inerter configurations. Inerters were also used in acoustic metamaterials to demonstrate bandgap widening via inertial amplification effect [34], seismic wave attenuation [35] or tuning of interface modes in elastic beam systems [36]. Topological interface states based on sub-wavelength in-plane waves were also studied in elastic metamaterials with translational resonators [20]. Moreover, in [37] the authors were able to form a band gap in the ultra-low frequency through inerters embedded into the matrix material.

Topological properties of sub-wavelength bands in the mass-in-mass locally resonant acoustic system were studied in [38] based on the spring-mass model and in [39] for a more complex structural acoustic-like system. The active control was also suggested to tune the interface states in a diatomic mass-in-mass acoustic metamaterial system having

nonlinear springs [40]. The analysis in the aforementioned works [38, 40] is confined to the diatomic-like locally resonant lattices with a limited number of non-trivial gaps and topologically protected edge/interface states. In [41], the authors have demonstrated the existence of several edge states in 1D polyatomic lattices with different cyclic permutations of springs and masses in the chain. Complex band structures and topological properties were obtained for different lattice configurations having multiple bands associated with higher winding numbers. However, the effect of local resonances on band structure and topological properties was not investigated in that study, which we aim to address in our work with special attention devoted to both diatomic-like and triatomic-like mass-in-mass lattices.

Topological properties of inerter-based lattices are less explored in the literature. In recent work [42], a new class of architected inertial metamaterials was suggested for 1D and 2D mechanical lattice design with novel topological and dispersion characteristics. However, most of the studies apply ideal inerter elements to represent the inertia amplification effect in mechanical systems. Such idealized properties is difficult to achieve in real inerter devices where damping and nonlinear effects are also present. In [43], different inerter-based hierarchical mechanical networks were considered in locally resonant flexural beams to study the effects of damping and inertance on wave propagation. A significant effect of damping on higher frequency interface modes of locally resonant phononic crystals was also observed in [44] based on theoretical and experimental analysis. Topological interface states are also realized in soft elastic metamaterials, which shown to be backscattering immune and robust to defects and changes in the environment [45]. However, as concluded in [46], due to their soft nature such metamaterials are having high damping ratio and propagation of elastic waves is possible only at short distances, which can also affect localized interface states. Therefore, consideration of damping can be crucial for reliable analysis of topological interface states in mechanical metamaterials and periodic structures.

In this work, we focused on the investigation of interface states in periodic damped inerter-based and locally resonant acoustic chains with diatomic-like and triatomic-like mass-in-mass unit cell configurations. To the best of the authors' knowledge, this is the first study to address such a topic with interesting findings regarding topological properties and the dynamic behaviour of specific types of one-dimensional mechanical lattices. First, dispersion analysis will be performed based on the free wave propagation in the bulk locally resonant acoustic lattice and then topological properties will be examined based on the topological invariant winding number and signs of the corresponding band gaps. The main reason for the investigation of bulk lattice topological properties in the momentum space is their connection to the existence of topological edge/interface states in finite lattices. Therefore, finite one-dimensional chains having two sub-lattices connected at the interface will be also considered and their dynamic behavior investigated. The influence of inerters and mass perturbation in local resonators on interface modes is compared based on the three illustrative examples of finite chains with different mass-in-mass unit cell configurations. Moreover, the effect of arbitrary viscous damping on steady-state responses of lattice outer mass points is investigated to reveal its effect on particular interface modes.

2. Wave dispersion and topology of ideal inerter-based lattices

In the seminal work by Smith [47], inerters were introduced as mechanical analogous to electrical networks. The basic idea of inerter elements in mechanical systems is to

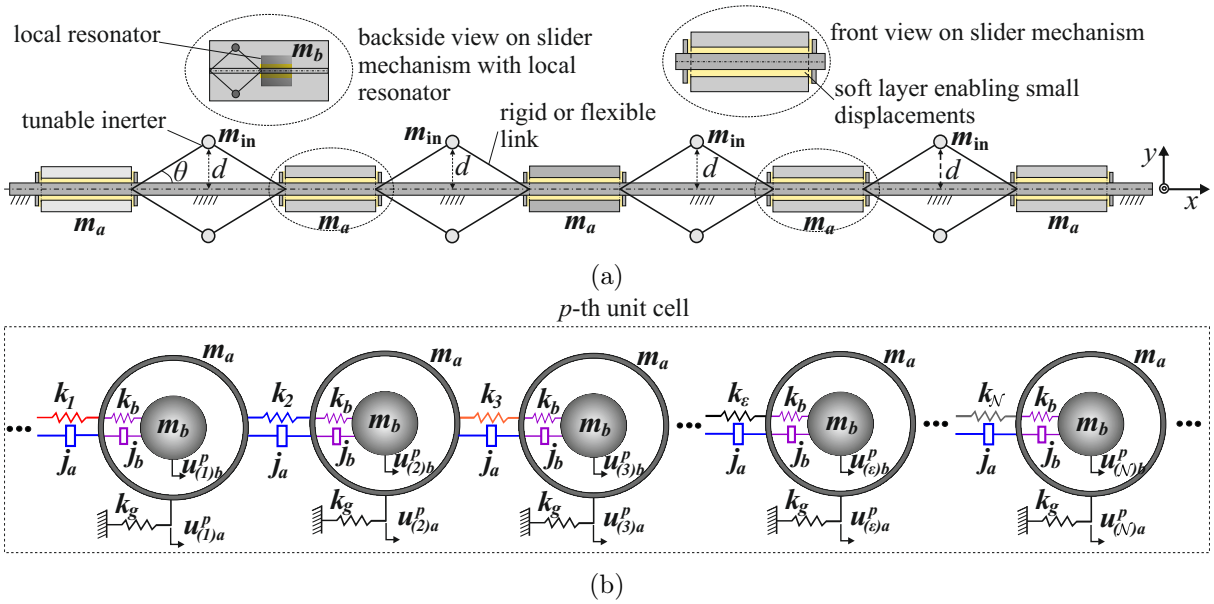

Fig. 1: One-dimensional inerter-based lattice with local resonators: (a) Illustration of the periodic slider mechanism with inerters based on lever-arms and secondary masses; (b) Equivalent mechanical model of a unit cell with $\mathcal{N}$ identical mass-in-mass subsystems and different springs connecting outer masses.

make a two-terminal device whose resistive force is proportional to the relative acceleration between the terminals. Such features can be achieved in many ways including pure mechanical [48], electromechanical [49], acoustic [50] or fluid-based inerters [51]. The force-displacement relationship of the ideal inerter is given as

$$F = b\,(\ddot{u}_2 - \ddot{u}_1) \tag{1}$$

where F is the resistive force, b is the inertance parameter and u_1 and u_2 are the displacements of two terminals. However, behavior of real inerter devices is far from ideal and different damping, hysteric or nonlinear effects need to be considered for accurate modelling [48].

A comprehensive study by Al Ba'ba'a et al. [42] explored the effect of inertance on both dispersion and topological characteristics of 1D and 2D architected inertial metamaterials (AIM). Special attention was devoted to ideal and linearized inerter-based infinite monoatomic AIM representing the lockable rigid slider system with tunable angle θ. The following relationship between the inertance and tunable angle was found $b = m(\tan^2\theta - 1)/4$, implying the values of $\theta \in (0, \pi/2]$ in order to satisfy the stability requirements (positive definite mass matrix). Similar linearized relationship was used in the work by Hussein et al. [52] for the inertially amplified metamaterials, where the effect of coupling of inertially amplified and local resonance attenuation peaks were investigated in detail. However, the aim of the analysis in this section is to reveal the effect of inertance and locally resonant mass on dispersion and topological characteristics of inerter-based mass-in-mass lattices while the effects of damping on interface states in finite locally resonant lattices will be elaborated in the following section.

Let us consider an infinitely long one-dimensional chain with a unit cell having $\mathcal{N}$ mass-in-mass subsystems that are mutually connected with different springs and inerter elements as illustrated in Figure 1b. This mechanical model could represent a real mechanical slider chain (see Figure 1a) with large masses mutually connected through inerters based on lever-arms and secondary masses (e.g. see [53]), where motions of these masses

(denoted with m_{in}) are supported by inclined lever arms with the angle of inclination θ. In that case, inertance parameters are calculated as $j_{a,b} = m_{\text{in}}/4\tan^2(\theta)$. Moreover, such a system can have both local resonators and inerters exhibiting the additional inertia amplification effect. Consideration of the soft layer foundation in the slider chain-like mechanism connecting the outer masses with the fixed base enables small displacements in the chain (Figure 1a). In the chain model from Figure 1b, we introduce ground springs of stiffness k_g, which represents a resistance of the soft layer to motion in the x direction. Under the assumption of small displacements and considering the ideal inerter elements, the motion equations of the p-th unit cell in the chain are given as

$$\begin{aligned} m_a\ddot{u}^p_{(\zeta)a} + (k_\zeta + k_{\zeta+1})\,u^p_{(\zeta)a} - k_\zeta u^p_{(\zeta-1)a} - k_{\zeta+1}u^p_{(\zeta+1)a} + k_b\left(u^p_{(\zeta)a} - u^p_{(\zeta)b}\right) + \\ j_a\left(2\ddot{u}^p_{(\zeta)a} - \ddot{u}^p_{(\zeta-1)a} - \ddot{u}^p_{(\zeta+1)a}\right) + j_b\left(\ddot{u}^p_{(\zeta)a} - \ddot{u}^p_{(\zeta)b}\right) + k_g u^p_{(\zeta)a} = 0, \end{aligned} \tag{2}$$

$$m_b\ddot{u}^p_{(\zeta)b} + k_b\left(u^p_{(\zeta)b} - u^p_{(\zeta)a}\right) + j_b\left(\ddot{u}^p_{(\zeta)b} - \ddot{u}^p_{(\zeta)a}\right) = 0, \tag{3}$$

where $\zeta = 2, 3, ..., \mathcal{N}-1$. The equations for the first mass-in-mass sub-system within the unit cell are given as

$$\begin{aligned} m_a\ddot{u}^p_{(1)a} + (k_1 + k_2)\,u^p_{(1)a} - k_1 u^{p-1}_{(\mathcal{N})a} - k_2 u^p_{(2)a} + k_b\left(u^p_{(1)a} - u^p_{(1)b}\right) + \\ j_a\left(2\ddot{u}^p_{(1)a} - \ddot{u}^{p-1}_{(\mathcal{N})a} - \ddot{u}^p_{(2)a}\right) + j_b\left(\ddot{u}^p_{(1)a} - \ddot{u}^p_{(1)b}\right) + k_g u^p_{(1)a} = 0, \end{aligned} \tag{4}$$

$$m_b\ddot{u}^p_{(1)b} + k_b\left(u^p_{(1)b} - u^p_{(1)a}\right) + j_b\left(\ddot{u}^p_{(1)b} - \ddot{u}^p_{(1)a}\right) = 0, \tag{5}$$

and for the last mass-in-mass sub-system in the unit cell as

$$\begin{aligned} m_a\ddot{u}^p_{(\mathcal{N})a} + (k_1 + k_\mathcal{N})\,u^p_{(\mathcal{N})a} - k_1 u^{p+1}_{(1)a} - k_\mathcal{N} u^p_{(\mathcal{N}-1)a} + k_b\left(u^p_{(\mathcal{N})a} - u^p_{(\mathcal{N})b}\right) + \\ j_a\left(2\ddot{u}^p_{(\mathcal{N})a} - \ddot{u}^{p+1}_{(1)a} - \ddot{u}^p_{(\mathcal{N}-1)a}\right) + j_b\left(\ddot{u}^p_{(\mathcal{N})a} - \ddot{u}^p_{(\mathcal{N})b}\right) + k_g u^p_{(\mathcal{N})a} = 0, \end{aligned} \tag{6}$$

$$m_b\ddot{u}^p_{(\mathcal{N})b} + k_b\left(u^p_{(\mathcal{N})b} - u^p_{(\mathcal{N})a}\right) + j_b\left(\ddot{u}^p_{(\mathcal{N})b} - \ddot{u}^p_{(\mathcal{N})a}\right) = 0, \tag{7}$$

where $u_{(\varepsilon)a}$ and $u_{(\varepsilon)b}$ for $\varepsilon = 1, 2, ..., \mathcal{N}$ are displacements of outer m_a and inner m_b masses, k_ε denotes stiffnesses of springs connecting outer masses, j_a is the inertance parameter of inerters connecting outer masses, k_b is the stiffness and j_b is the inertance of local resonators while k_g is the stiffness of ground springs. We remark that the last outer mass in the unit cell is connected to the next unit cell through the spring $k_{\mathcal{N}+1} = k_1$. We should also emphasize that values of outer and inner masses, inerter parameters, and stiffness of inner mass springs are the same throughout the unit cell while only stiffness of springs connecting outer masses can be varied.

Based on the Bloch theorem and boundary conditions for the unit cell, we can write the following relation for the displacements of the ending outer masses

$$u^{p\mp1}_{(1,\mathcal{N})a} = u^p_{(\mathcal{N},1)a}\exp(\mp\mathrm{i}\mu), \tag{8}$$

with μ denoting the dimensionless wave number and $\mathrm{i} = \sqrt{-1}$. After assuming the harmonic solution as $u^p_{(\varepsilon)a,b}(t) = \hat{u}_{(\varepsilon)a,b}(\omega)\exp(\mathrm{i}\omega t)$, one can obtain the matrix equation for the p-th unit cell in the following form

$$\mathbf{D}_p(\omega,\mu)\hat{\mathbf{u}} = \mathbf{0}, \tag{9}$$

where $\hat{\mathbf{u}}^T = \left[\hat{u}_{(1)a}, \hat{u}_{(1)b}, ..., \hat{u}_{(\mathcal{N})a}, \hat{u}_{(\mathcal{N})b}\right]_{2\mathcal{N}}$ and $\mathbf{D}_p(\omega,\mu)$ is the dynamic stiffness matrix that is given as

$$\underset{2\mathcal{N}\times 2\mathcal{N}}{\mathbf{D}_p}(\omega,\mu) = \mathbf{K}_p(\mu) - \omega^2\mathbf{M}_p(\mu) \tag{10}$$

where we have

$$\mathbf{M}_p = \mathbf{M}^m_p + \mathbf{M}^b_p, \tag{11}$$

$$\mathbf{M}^m_p = \mathbf{diag}\left[m_a, m_b, m_a, m_b, ..., m_a, m_b\right], \tag{12}$$

$$\mathbf{M}^b_p(\mu) = \begin{bmatrix} 2j_a+j_b & -j_b & -ja & 0 & \cdots & 0 & -j_a e^{-\mathrm{i}\mu} & 0 \\ -j_b & j_b & 0 & \cdots & \cdots & \cdots & \cdots & 0 \\ -ja & 0 & 2j_a+j_b & -j_b & -j_a & 0 & \cdots & \vdots \\ 0 & 0 & -j_b & j_b & 0 & \ddots & \ddots & \vdots \\ \vdots & \ddots & \ddots & \ddots & \ddots & \ddots & \ddots & \vdots \\ 0 & \ddots & \ddots & \ddots & \ddots & \ddots & \ddots & 0 \\ -j_a e^{\mathrm{i}\mu} & 0 & \cdots & 0 & -j_a & 0 & 2j_a+j_b & -j_b \\ 0 & \cdots & \cdots & \cdots & \cdots & 0 & -j_b & j_b \end{bmatrix}, \tag{13}$$

and

$$\mathbf{K}_p(\mu) = \begin{bmatrix} \sum_{u=1}^{2} k_u+k_b+k_g & -k_b & -k_2 & 0 & \cdots & 0 & -k_{\mathcal{N}} e^{-\mathrm{i}\mu} & 0 \\ -k_b & k_b & 0 & \cdots & \cdots & \cdots & \cdots & \vdots \\ -k_2 & 0 & \sum_{u=2}^{3} k_u+k_b+k_g & -k_b & -k_3 & 0 & \cdots & \vdots \\ 0 & 0 & -k_b & k_b & 0 & \ddots & \ddots & \vdots \\ \vdots & \ddots & \ddots & \ddots & \ddots & \ddots & \ddots & \vdots \\ 0 & \ddots & \ddots & \ddots & \ddots & \ddots & \ddots & 0 \\ -k_1 e^{\mathrm{i}\mu} & 0 & \cdots & 0 & -k_{\mathcal{N}} & 0 & k_{\mathcal{N}}+k_1+k_b+k_g & -k_b \\ 0 & \cdots & \cdots & \cdots & \cdots & 0 & -k_b & k_b \end{bmatrix}. \tag{14}$$

By setting the determinant of the above dynamic stiffness matrix equal to zero, one can obtain the characteristic equation and corresponding eigenvalues in terms of the dimensionless wavenumber. This enables us to plot dispersion curves for the suggested unit cell configuration and determine the band structure. To characterize the topology of eigenvectors associated with the corresponding bands we employ the topological invariant named Zak phase [19], which for the m-th band is calculated as

$$\theta^{\mathrm{Zak}}_{(m)} = \mathrm{i}\int_{-\pi}^{\pi}\left[\hat{\mathbf{u}}^H_m(\mu)\cdot\partial_\mu\hat{\mathbf{u}}_m(\mu)\right]\mathrm{d}\mu, \tag{15}$$

where $\hat{\mathbf{u}}^H_m(\mu)$ is the Hermitian of the eigenvector $\hat{\mathbf{u}}_m(\mu)$. However, for the numerical calculations of the Zak phase in this study we use the discretized form of the equation [19] that is given as

$$\theta^{\mathrm{Zak}}_{(m)} = -\mathrm{Im}\sum_{n=-N_s}^{N_s-1}\ln\left[\hat{\mathbf{u}}^H_m(\frac{n}{N_s}\pi)\cdot\hat{\mathbf{u}}_m(\frac{n+1}{N_s}\pi)\right], \tag{16}$$

where N_s is the number of discretization steps. In general, Zak phase takes the values of $\theta_{(m)}^{\text{Zak}} = 0$ and $\theta_{(m)}^{\text{Zak}} = \pi$, which is also related to another topological invariant called winding number $w = \theta_{(m)}^{\text{Zak}}/\pi (\text{mod } 2)$ that will take the values $w = 0$ and $w = 1$, respectively. However, as given in [54], this is not always true for generic multi-band systems (SSH chains), where one can distinguish the so-called intracellular and intercellular Zak phase, since the contribution of phase from a band may take larger values such as $\theta_{(m)}^{\text{Zak}} = 2\pi$, which also affects the winding numbers. Further, if we form a block of two lattices with a unique band structure, the major requirement to have a topologically protected interface state within some n-th band gap is that they have bands with different topologies. According to [55], interface states in 1D phononic crystals (PCs) with inversion symmetry can be characterized by summing all Zak phases below the gap. Based on the bulk-interface correspondence principle, which is equivalent to the bulk-edge correspondence in topological insulators, they proposed the sign of the impedance as a measure for the existence of interface states in PCs. More precisely, if the signs of some n-th gap of the lattices on opposite sides of the interface are different, then that band gap is characterized as topologically non-trivial. The sign of the n-th band gap can be determined based on the following relation

$$\text{sign}[\zeta^{(n)}] = (-1)^n (-1)^l \exp\left[i \sum_{m=1}^{n} \theta_{(m)}^{\text{Zak}} \right], \tag{17}$$

where numeration is executed such that the lowest frequency (1st) band is $m = 1$, while the 1st band gap $n = 1$ is the one above the 1st band (zero-frequency gap starting at zero and cutoff, while the frequency of the first band is not considered). Note, that l denotes the number of crossing points below the gap, where the entire term can be neglected ($l = 0$) if there are no crossings. This section provides the framework to investigate topological characteristics of diatomic-like and triatomic-like mass-in-mass unit cell configurations and reveal the influence of ideal inerters on band topology.

3. Finite inerter-based lattices with damping

From the preceding theoretical analysis one can investigate elastic wave dispersion and topological properties of 1D inerter-based diatomic- and triatomic-like chains with a local resonator. Based on the assumption of infinite lattices, one can discover whether they support topologically protected interface modes at the interface between the two lattice types or not. In practice, only the finite lattices can be realized and the existence of interface states is confirmed through the eigenvalue and frequency response function analysis. However, apart from the dispersion properties, such large periodic systems will always exhibit some kind of dissipation, especially when inerter devices are embedded into the lattice. Here, we attempt to extend the theoretical investigation by including the viscous dissipation effect through the mechanical model representing the electromagnetic damper (EMD). For example, in [43] the authors considered different mechanical networks involving spring, dashpot, and inerter elements to represent mechanical inerters in an elastic beam system with local resonators. Recently, in [56] the authors proposed a motor-based EMD in a mechanical system capable to perform as both a damper and energy-harvesting device. This EMD mainly consists of a motor and a ball-screw (see Figure 2a) and it forms a two-terminal device whose resisting force is defined as

$$F = b\left(\ddot{u}_2 - \ddot{u}_1\right) + c_{eq}\left(\dot{u}_2 - \dot{u}_1\right) \tag{18}$$

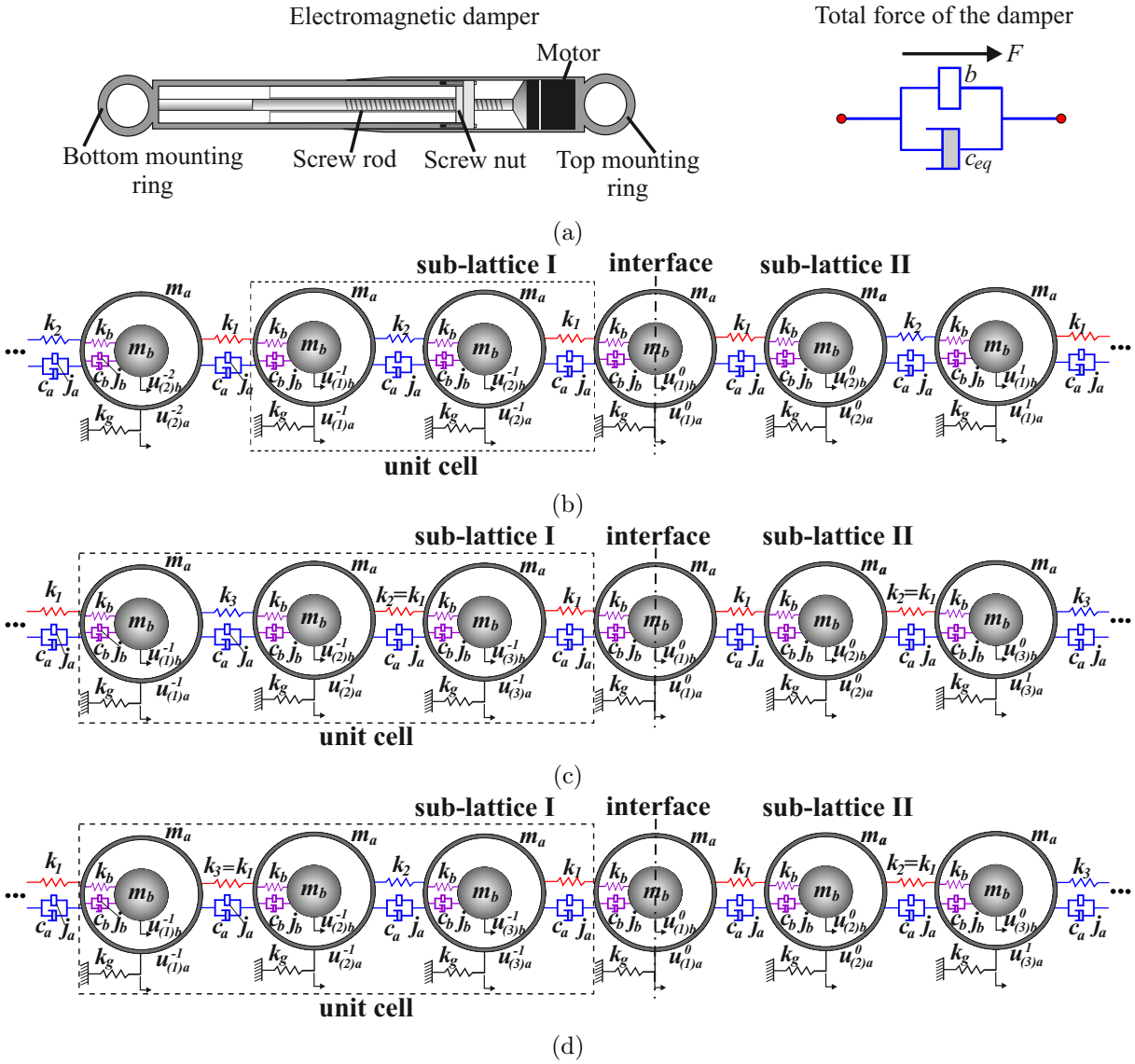

Fig. 2: Damped inerter-based one-dimensional finite diatomic-like and triatomic-like mass-in-mass chains: (a) Illustration of the electromagnetic damper (e.g. see [56]); (b) Block of two connected sub-lattices having diatomic-like mass-in-mass unit cells and outer springs defined as $k_1 = k(1+\gamma)$ and $k_2 = k(1-\gamma)$; (c) Block of two connected sub-lattices having triatomic mass-in-mass unit cells and outer springs defined as $k_1 = k(1+\gamma)$, $k_2 = k_1$ and $k_3 = k(1-\gamma)$; (d) Block of two connected sub-lattices having triatomic mass-in-mass unit cells and outer springs defined as $k_1 = k(1+\gamma)$, $k_2 = k(1-\gamma)$ and $k_3 = k_1$ in the sub-lattice I and $k_1 = k(1+\gamma)$, $k_2 = k_1$ and $k_3 = k(1-\gamma)$ in the sub-lattice II.

where $b = J(4\pi^2/l^2)$ is the inertance, J is the sum of moments of inertia of EMD, l is the lead of the ball-screw and $c_{eq} = c_{eq}(2\pi/l)^2$ is the linear equivalent viscous damping coefficient with c_{eq} denoting the rotary damping coefficient of the motor. Here, we will employ this phenomenological model to represent the resistive forces of mechanical inerters (or EMDs) embedded into the diatomic- and triatomic-like chains with local resonators.

The finite inerter-based one-dimensional mass-in-mass chains with interface and three different types of unit cells are illustrated in Figure 2. The chain is formed as a block of two sub-lattices connected at the interface, which can be but not necessarily inverted copies of each other. In general case, the outer masses are mutually connected through springs with different stiffness coefficients k_1 and k_2 for diatomic-like lattices and k_1, k_2

and k_3 for the triatomic-like lattices and parallelly connected inerter elements of inertance j_a and dashpot elements with viscous damping coefficient c_a. The stiffness k_b, inertance j_b and viscous damping coefficient c_b are related to inner mass local resonators. Note that the choice of unit cells and numeration of outer springs for both sub-lattices in the chain is different from the one given in the previous section (see Figure 2 for details). First, we write the motion equations of the diatomic-like mass-in-mass chain. By following the notation from Figure 2b, we can write four motion equations for the r-th mass-in-mass subsystem in the p-th unit cell of the sub-lattice I on the left side of the interface as

$$\begin{aligned} m_a\ddot{u}^p_{(r)a} + j_a\left(2\ddot{u}^p_{(r)a} - \ddot{u}^p_{(k)a} - \ddot{u}^{p+P}_{(k)a}\right) + j_b\left(\ddot{u}^p_{(r)a} - \ddot{u}^p_{(r)b}\right) + c_b\left(\dot{u}^p_{(r)a} - \dot{u}^p_{(r)b}\right) + \\ c_a\left(2\dot{u}^p_{(r)a} - \dot{u}^p_{(k)a} - \dot{u}^{p+P}_{(k)a}\right) + k_2\left(u^p_{(r)a} - u^p_{(k)a}\right) + \\ k_1\left(u^p_{(r)a} - u^{p+P}_{(k)a}\right) + k_b\left(u^p_{(r)a} - u^p_{(r)b}\right) + k_g u^p_{(r)a} = 0, \end{aligned} \tag{19}$$

$$m_b\ddot{u}^p_{(r)b} + j_b\left(\ddot{u}^p_{(r)b} - \ddot{u}^p_{(r)a}\right) + c_b\left(\dot{u}^p_{(r)b} - \dot{u}^p_{(r)a}\right) + k_b\left(u^p_{(r)b} - u^p_{(r)a}\right) = 0. \tag{20}$$

where subscript indices are defined as $r, k = 1, 2$ for $r \neq k$ and $P = 1$ for $r = 1$ while $P = -1$ for $r = 2$. The equations for the sub-lattice II on the right side of the interface can be written in the same manner where only springs k_1 and k_2 swap their places.

For the triatomic-like chain, the motion equations for the r-th mass-in-mass subsystem of the p-th unit cell in the sub-lattice I are given as

$$\begin{aligned} m_a\ddot{u}^p_{(r)a} + j_a\left(2\ddot{u}^p_{(r)a} - \ddot{u}^{p+P}_{(k)a} - \ddot{u}^p_{(s)a}\right) + j_b\left(\ddot{u}^p_{(r)a} - \ddot{u}^p_{(r)b}\right) + c_b\left(\dot{u}^p_{(r)a} - \dot{u}^p_{(r)b}\right) + \\ c_a\left(2\dot{u}^p_{(r)a} - \dot{u}^{p+P}_{(k)a} - \dot{u}^{p+P}_{(s)a}\right) + k_{(m)}\left(u^p_{(r)a} - u^{p+P}_{(k)a}\right) + \\ k_{(n)}\left(u^p_{(r)a} - u^p_{(s)a}\right) + k_b\left(u^p_{(r)a} - u^p_{(r)b}\right) + k_g u^p_{(r)a} = 0, \end{aligned} \tag{21}$$

$$m_b\ddot{u}^p_{(r)b} + j_b\left(\ddot{u}^p_{(r)b} - \ddot{u}^p_{(r)a}\right) + c_b\left(\dot{u}^p_{(r)b} - \dot{u}^p_{(r)a}\right) + k_b\left(u^p_{(r)b} - u^p_{(r)a}\right) = 0. \tag{22}$$

with subscript indices defined as $r, k, s, n, m = 1, 2, 3$ (note that indices n and m do not refer to the band's or gap's numbers), $r \neq k \neq s$, $n \neq m$, where for $r = 1$ we have that $m = 1$, $n = 3$, $k = 3$, $s = 2$, $P = -1$ for $r = 2$ we have $m = 3$, $n = 2$, $k = 1$, $s = 3$, $P = 0$ and for $r = 3$ we have $m = 1$, $n = 2$, $k = 1$, $s = 2$, $P = 1$. For the convenience we adopted that $k_{(1)} \equiv k_1$, $k_{(2)} \equiv k_2$ and $k_{(3)} \equiv k_3$. The equations for the mass-in-mass sub-system in the sub-lattice II can be obtained if we swap the places of the springs k_1 and k_3. These equations are valid for both triatomic-like mass-in-mass configurations from Figures 2c and 2d, where only corresponding equal stiffness springs in the sub-lattice I and II should be applied to obtain the corresponding finite lattice equations.

The equations of motion of a viscously damped finite diatomic-like and triatomic-like chains with some external excitation can be also written in the compact matrix form as

$$\mathbf{M}\ddot{\mathbf{q}}(t) + \mathbf{C}\ddot{\mathbf{q}}(t) + \mathbf{K}\mathbf{q}(t) = \mathbf{f}(t), \tag{23}$$

where vector $\mathbf{q}$ for the diatomic-like mass-in-mass lattice is given as

$$\mathbf{q} = \left[u^{-N}_{(2)a}, u^{-N}_{(2)b}, u^{-N+1}_{(1)a}, u^{-N+1}_{(1)b}, ..., u^{0}_{(1)a}, u^{0}_{(1)b}, ..., u^{N}_{(2)a}, u^{N}_{(2)b}\right], \tag{24}$$

while for the triatomic-like mass-in-mass lattice we have

$$\mathbf{q} = \left[u_{(1)a}^{-N}, u_{(1)b}^{-N}, u_{(2)a}^{-N}, u_{(2)b}^{-N}, u_{(3)a}^{-N}, u_{(3)b}^{-N}..., u_{(1)a}^{0}, u_{(1)b}^{0}, u_{(2)a}^{0}, u_{(2)b}^{0}, ..., u_{(3)a}^{N}, u_{(3)b}^{N}\right], \tag{25}$$

where $\mathbf{M}$ is the mass matrix, $\mathbf{C}$ is the damping matrix and $\mathbf{K}$ is the stiffness matrix, which are obtained based on Eqs. 19 - 22 for the mass-in-mass unit cells of diatomic-like and triatomic-like chains with local resonators. The solution procedure of Eq. 23 and steady-state responses of lattice points in arbitrary viscous damping case is given in Appendix A. Damped response will be utilized in the next section to investigate its effect on interface states. Further, by neglecting the excitation force and damping terms and assuming the solution of the form $\mathbf{q}(t) = \tilde{\mathbf{q}}e^{\mathrm{i}\Omega t}$ one can determine the natural frequencies of the finite undamped chain by finding the eigenvalues of the following characteristic equation

$$\det\left(\mathbf{K} - \Omega^2\mathbf{M}\right) = 0. \tag{26}$$

By using the above equations one can also compute the frequency response function (FRF) to illustrate the dynamic behaviour of the chain. To test whether finite lattices support interface modes, three different cases with corresponding boundary conditions will be considered in this study. The first case includes a diatomic-like mass-in-mass unit cell with alternating springs k_1 and k_2 in the lattices on the left and right side of the interface (Figure 2b). The second case includes triatomic-like lattices on both sides of the interface, where springs k_1 and k_2 are equal $k_1 = k_2$ while k_3 is different in the sub-lattices I and II that are mirror-like images (different from the mirror symmetry in the sub-lattice unit cell) of each other, Figure 2c. The third example considers the case where $k_1 = k_3$ in the sub-lattice I and $k_1 = k_2$ in the sub-lattice II Figure 2d. Therefore, in all considered cases there are only two different stiffness springs in the sub-lattice unit cell connecting the outer masses that can take either the value $k(1 + \gamma)$ or $k(1 - \gamma)$, where k is the mean stiffness and γ is the dimensionless stiffness parameter. Note that numerations of outer springs in the finite chain sub-lattices are different from those given in the previous section and also $\gamma = 0$ will result in all equal springs in the lattice. Therefore, dispersion analysis of diatomic- or triatomic-like chain unit cells on different sides of the interface would result in the same band structures but different topology, which is an important condition to study the existence of interface states in finite lattices. In the following, to study the finite diatomic-like and triatomic-like mass-in-mass chains with local resonators we consider $p = 2N$ unit cells (with numeration $p = [-N, ..., -1, 0, 1..., N]$), thus, having N unit cells in each of the two sub-lattices.

4. Discussion and numerical results

Investigating the band structure and topological properties of periodic lattices can give us important information about the occurrence of topologically protected interface states. It is well known that diatomic and certain polyatomic unit cell configurations for different cyclic or non-cyclic permutations can have identical band structures but different topological properties of eigenvectors [9]. In such lattices one can notice "twisting" of eigenvectors in sign since some of the branches attempt to localise deformations at softer springs and thus leaving the stiffer ones undeformed. In the literature, this phenomenon is called band inversion. Another important sign of the band inversion is the process of band gap closing/opening for certain values of parameters in the unit cell (band-folding induced band gaps). In our case, band gap closing occurs when different springs in the unit cell are having equal stiffness. Important metrics for measuring topological properties

of one-dimensional solids is the geometrical phase called Zak's phase. Normalisation of Zak's phase by the unit π yields the so-called winding number (here denoted as w) that actually quantifies the number of times certain eigenvector winds around the origin of the complex plane in the momentum space. It should be noted that the Zak phase is not always quantized (equal to π) due to its dependence on the unit cell symmetry, which also means that the winding number is not necessarily an integer [41].

In the first part of our numerical study we will investigate dispersion and topological characteristics of diatomic-like and triatomic-like mass-in-mass unit cells with and without inerters based on the equations presented in Section 2. This will give us an important information for interpretation of topological properties of band gaps in adopted lattice configurations. The second and third part of the numerical study shows the dynamic behaviour of finite lattices with existing interface states as well as the effect of non-proportional viscous damping on particular interface modes. We remark that, in all given numerical examples, natural frequency is normalised by the local resonance frequency of the internal resonator (frequency of the initial configuration without inerters and changes in the locally resonant mass), which is given as $\omega_b = \sqrt{k_b/m_b}$. The following values of parameters are used in simulations if not given otherwise in figures: $k = 10000$ N/m, $k_b = 8000$ N/m, $k_g = 3000$ N/m, $m_a = 1$ kg, $m_b = 0.5$ kg.

4.1. Dispersion and topological properties of inerter-based lattices with local resonators

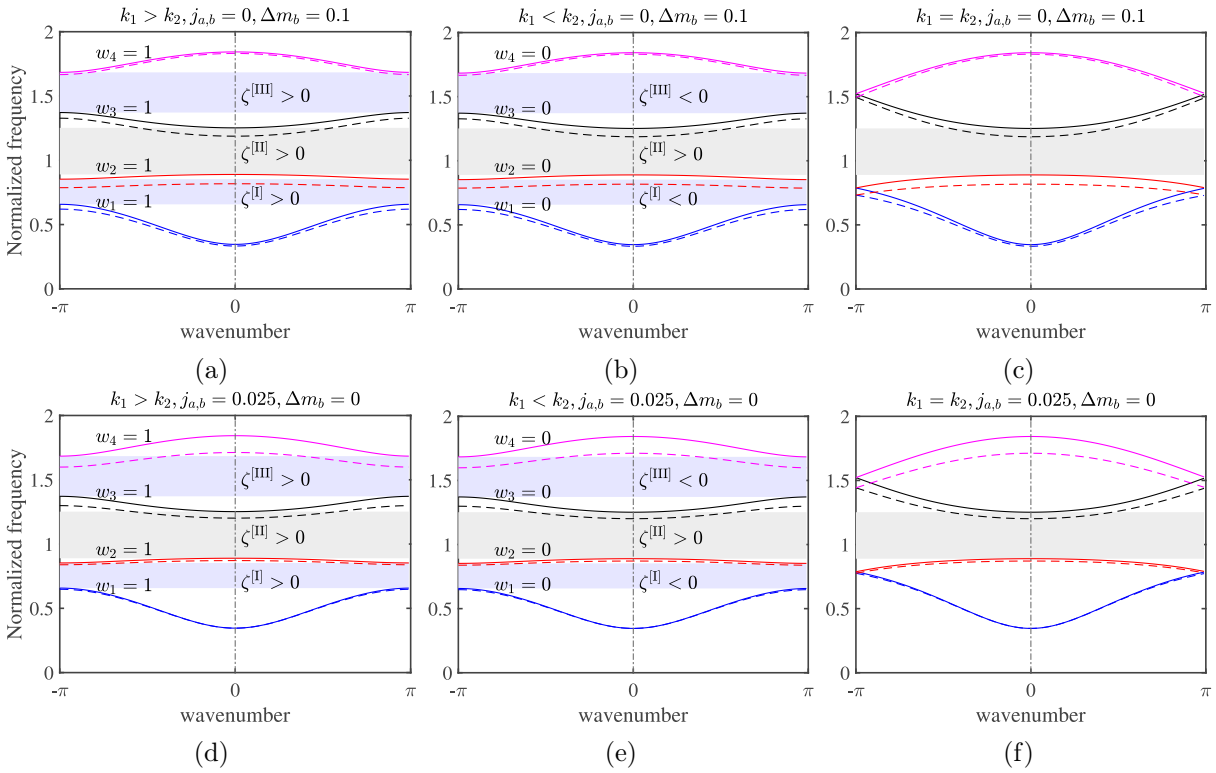

Fig. 3: Comparison of the tuning effect of local resonators and inerters on dispersion and topological characteristics of the diatomic-like mass-in-mass unit cell with springs $k_1 = k(1+\gamma)$ and $k_2 = k(1-\gamma)$ when $\gamma = 0.5$, $\gamma = -0.5$ and $\gamma = 0$ (from left to right). The panels (a)-(c) refers to the lattices without inerters when $m_b = m_{b(0)}$ (solid lines) and with change $\Delta m_b = 0.1$ in locally resonant mass according to $m_b = m_{b(0)} + \Delta m_b$ (dashed lines). The panels (d)-(f) refers to the lattices without (solid lines) and with inerters $j_{a,b} = 0.025$ (dashed lines) and no change in locally resonant mass $m_b = m_{b(0)}$.

Here we investigate the dispersion and topological properties of inerter-based lattices with diatomic-like and triatomic-like mass-in-mass unit cells. Special attention is devoted to infinite lattices that satisfy the unit cell mirror symmetry condition, which in analogy to the simple diatomic and some triatomic lattices [41] means that neighboring cells from two sides of the mirror are reciprocal arrangements of one another, which in the case of diatomic-like and triatomic-like mass-in-mass unit cells can be achieved when there are only two different outer springs in the lattice. This feature is crucial to achieving the quantized Zak phase. For that purpose, in Eq. 10 of the diatomic-like mass-in-mass unit cell we use springs $k_1 = k(1+\gamma)$ and $k_2 = k(1-\gamma)$ with k denoting the mean stiffness, while for the triatomic-like mass-in-mass unit cell we have $k_1 = k(1+\gamma)$, $k_2 = k(1-\gamma)$ and $k_3 = k_2$. In this section, to obtain realistic values of inertance that are related to the rigid lever-arms like inerter mechanism (Figure 1a), we use the following equation $j_{a,b} = m_{\text{in}}/4\tan^2(\theta)$, where m_{in} and θ are inerter's mass and inclination angle, respectively. For the sake of simplicity, the inerter parameters j_a and j_b are considered to be the same and given in units of kilograms, where their values are calculated for the inclination angle $\theta = 43°$ and small values of inerter's secondary mass $m_{\text{in}} = 0.1$ kg.

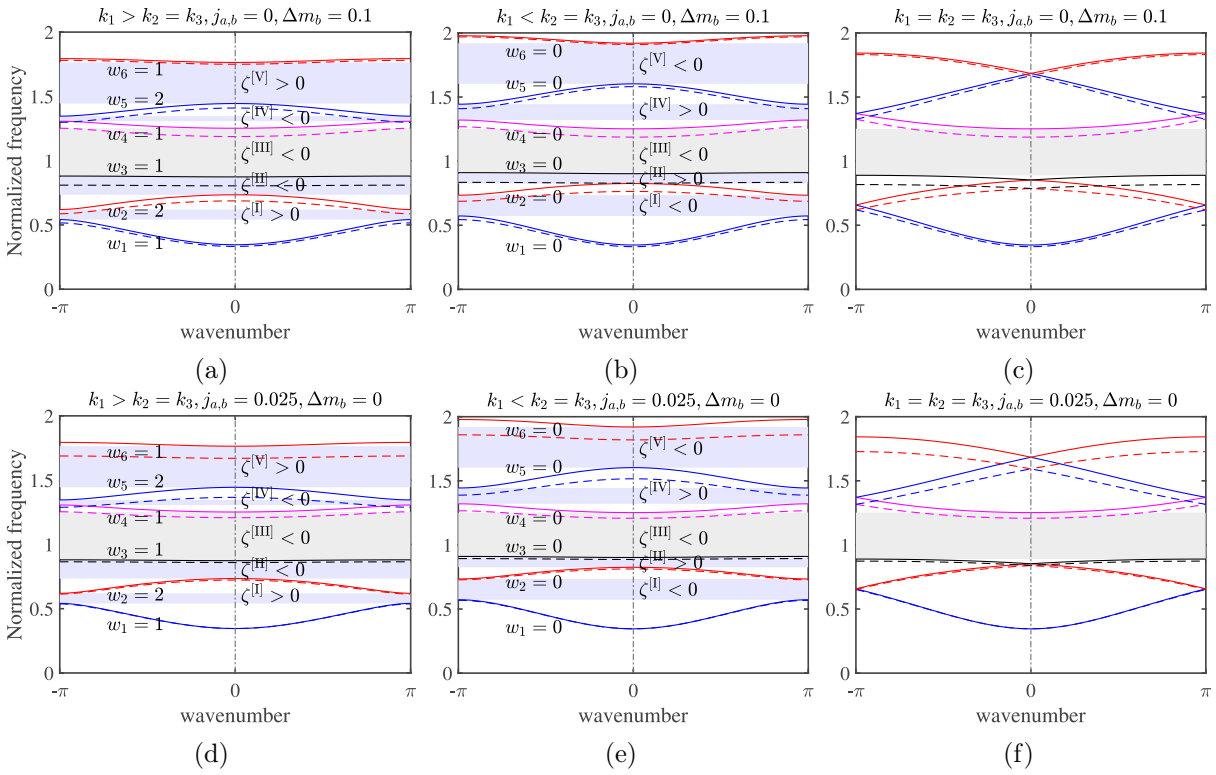

Fig. 4: Comparison of the tuning effect of local resonators and inerters on dispersion and topological characteristics of the triatomic-like mass-in-mass unit cell with springs $k_1 = k(1+\gamma)$, $k_2 = k(1-\gamma)$ and $k_3 = k_2$ when $\gamma = 0.5$, $\gamma = -0.5$ and $\gamma = 0$ (from left to right). The panels (a)-(c) refers to the lattices without inerters when $m_b = m_{b(0)}$ (solid lines) and with change $\Delta m_b = 0.1$ in the locally resonant mass according to $m_b = m_{b(0)} + \Delta m_b$ (dashed lines). The panels (d)-(f) refers to the lattices without (solid lines) and with inerters $j_{a,b} = 0.025$ (dashed lines) and no change in locally resonant mass $m_b = m_{b(0)}$.

It is well known that local resonators can be used in periodic lattices to shift bands and consequently band gaps to lower frequencies, especially in the sub-wavelength range. Graded design of local resonators can significantly enhance the tunability properties of such lattices [57]. However, embedded inerter elements into 1D lattices will introduce some new but different band tuning variables. In the following analysis, the effects of

both local resonators and inerters on dispersion and topological properties of 1D lattices will be compared. Figure 3 shows dispersion curves, corresponding winding numbers, and signs of band gaps of diatomic mass-in-mass unit cells with and without inerters and with small perturbations in locally resonant masses. Solid lines states for the unchanged (initial) configuration of the lattice without inerters and unchanged inner masses of local resonators while dashed lines refer to changed configurations. Moreover, parameter γ is varied as $\gamma = 0.5$ ($k_1 > k_2$), $\gamma = -0.5$ ($k_1 < k_2$) to show the band structures of the lattices with different spring stiffness variations. It should be noted that the folded dispersion diagram of Figure 3c and Figure 3f corresponds to the case where $\gamma = 0$ ($k_1 = k_2$), so that band-folding induced gaps are opening for $\gamma \neq 0$. Same band structures with four bands and three band gaps but different topology and quantized topological invariant are obtained for $\gamma = 0.5$ and $\gamma = -0.5$. The first three panels (Figure 3 (a)-(c)) refers to the case without inerters where only mass of the local resonator is increased for $\Delta m_b = 0.1$ according to $m_b = m_{b(0)} + \Delta m_b$, where $m_{b(0)}$ is the locally resonant mass in initial configuration. Here, shifting of frequency to lower values can be noticed in both higher and lower frequency bands (dashed lines). However, this shifting is much more pronounced in the lower frequency bands, which is in line with the previous findings in the literature. Next three panels (Figure 3 (d)-(f)) refers to the case of inerter-based lattice with inertance $j_a = j_b = 0.025$ calculated according to the previously given formula and corresponding to the inerter's secondary mass $m_{\text{in}} = 0.1$. In this case, shifting of bands (dashed line) to lower frequency values can be noticed in all bands but changes are much more pronounced in the higher frequency bands. This influence is opposite to the influence of local resonators that mostly affect the lower frequency bands. By observing the band structure, one can notice three band gaps whose topological properties are determined based on Eq. 17 and indicated in figures as $\zeta^{(n)} \lessgtr 0$, where $n = \text{I, II, II}$ is the gap number (excluding the zero-frequency gap). The observation shows that band gaps of both initial and changed lattice configurations are having the same topological properties. This fact is important from the viewpoint of the capability of inerter-based locally resonant lattices to tune interface modes without changing the topological properties of the initial lattice configuration without inerters. Further, a comparison of non-trivial and trivial topological properties of individual bands and band gaps gives us important information for the possible existence of interface states within the band gaps of the two lattice types with different topology. The obtained results shows that all the bands are having quantized Zak's phase indicated by the integer winding numbers with the values $w_m = 0$ or $w_m = 1$ for $k_1 < k_2$ and $k_1 > k_2$, respectively. However, observation of band gap topology through the sign of ζ^n shows that only gaps I and III are non-trivial due to the opposite signs while gap II is the trivial one (same signs for both lattice types). This means that non-trivial interface states will exist in the long chain, constructed from the two lattice types ($k_1 < k_2$ and $k_1 > k_2$), only within the gaps I and III. The second gap remains the same through all three band structure examples indicating its locally resonant origin and trivial topology nature, which is in line with the previous findings by other authors [38].

Further, Figure 4 shows dispersion curves and topological properties of bands and corresponding band gaps of the triatomic mass-in-mass unit cells with and without inerters. The case with three springs $k_1 = k(1+\gamma)$, $k_2 = k(1-\gamma)$ and $k_3 = k_2$ is studied, i.e. only one spring connecting the outer masses is different from others. This configuration is adopted in analogy to the simple triatomic unit cell with mirror symmetry and quantized Zak's phase. It should be noted that mirror symmetry within the bulk lattice with triatomic mass-in-mass unit cells, when masses are equal, can be achieved only when one of the springs in the unit cell is different from the others (see [41]). Band structure shows

Table 1: Sign $\zeta^{(n)}$ of the n-th band gap for the diatomic-like and triatomic-like unit cells with local resonators and inerters. The band gaps of triatomic-like mass-in-mass unit cell configurations with bands having *non-quantized* Zak's phase are indicated with *NQ*.

	Diatomic mass-in-mass		Triatomic mass-in-mass			
	$k_1 > k_2$	$k_1 < k_2$	$k_1 > k_2 = k_3$	$k_1 < k_2 = k_3$	$k_3 \lesseqgtr k_1 = k_2$	$k_2 \lesseqgtr k_1 = k_3$
$\mathrm{sgn}[\zeta^{(\mathrm{I})}]$	$+$	$-$	$+$	$-$	NQ	NQ
$\mathrm{sgn}[\zeta^{(\mathrm{II})}]$	$+$	$+$	$-$	$+$	NQ	NQ
$\mathrm{sgn}[\zeta^{(\mathrm{III})}]$	$+$	$-$	$-$	$-$	NQ	NQ
$\mathrm{sgn}[\zeta^{(\mathrm{IV})}]$			$-$	$+$	NQ	NQ
$\mathrm{sgn}[\zeta^{(\mathrm{V})}]$			$+$	$-$	NQ	NQ

six bands and five band gaps (excluding the zero-frequency band gap) in both unit cell configurations with and without inerters. However, the band structures of the lattices in the configuration $\gamma = -0.5$ and $\gamma = 0.5$ are distinct due to the obvious change in the overall stiffness and different gap opening after the band-folding case $\gamma = 0$. Here, we again compare the effects of change of the locally resonant mass and inerter elements on the dispersion and topological behavior of the lattice. The dashed lines in the first three panels (Figure 4 (a)-(c)) refers to the lattice with Δm_b change in locally resonant mass according to $m_b = m_{b(0)} + \Delta m_b$, while the initial lattice configuration without inerters and locally resonant mass given as $m_b = m_{b(0)} = 0.5$ is indicated by solid lines. It can be observed that an increase of the locally resonant mass shifts all the bands to lower frequencies. This shifting is more pronounced for the lower frequency bands, same as in the case of diatomic-like mass-in-mass lattices. On the other hand, the effect of introduced inerters with inertance parameters $j_{a,b} = 0.025$ is the opposite, where the most affected are the higher frequency bands when compared to the initial lattice configuration (Figure 4 (d)-(f)). The topological properties of individual bands are indicated by the winding numbers that can take value $w = 0$ corresponding to $\theta_m^{\mathrm{Zak}} = 0$ or integer values $w = 1$ and $w = 2$ corresponding to $\theta_m^{\mathrm{Zak}} = \pi$ and $\theta_m^{\mathrm{Zak}} = 2\pi$, respectively. One can notice that the second and fifth bands are having winding numbers $w = 2$, which means that corresponding complex eigenvectors are "wrapping" twice around the center of the complex plane. According to [58] quantized Zak's phase can take only the values of 0 and π owing to the modulo of 2π, which would possibly require modification of Eq. 17 for the sign of band gaps. However, Eq. 17 can still be used in its present form since for the higher values of the Zak phase a contribution of additional π in the geometric phase also takes into account corresponding change in the sign (double winding of the eigenvectors). Further, different signs of $\zeta^{(n)}$ for the gaps I, II, IV, and V in two lattice configurations $\gamma = -0.5$ and $\gamma = 0.5$ demonstrates the non-trivial nature of these band-folding induced band gaps. Though the size of gap III seems to remain the same through all three band structure examples, a change in the frequency of all bands and band gaps size occurs between the configurations $\gamma = 0.5$ and $\gamma = -0.5$ owing to the obvious difference in the overall stiffness (there is an odd number of outer springs). However, this is the only gap that has the same signs of $\zeta^{(n)}$ for both lattices, $\gamma = -0.5$ and $\gamma = 0.5$, indicating its trivial topology. The results demonstrate the potential of inerters to significantly tune the band gaps and corresponding interface states with very small secondary masses of the inerter's mechanism. This inertia amplification effect can be even more enhanced for a smaller inclination angle ($\theta < 43^\circ$) of the inerter and the same secondary mass. Moreover,

a combined effect of perturbations in locally resonant mass and inerters' parameters can, even more, contribute to tuning capabilities of the inerter-based locally resonant lattices in both higher and lower frequency bands, while keeping the main topological properties of the initial configuration without inerters.

Finally, Table 1 shows the sign of $\zeta^{(n)}$ for different band gaps of the diatomic-like and triatomic-like mass-in-mass unit cells for all possible permutations of springs k_1, k_2 and k_3 connecting outer masses when only one spring is different from others. The table outlines the previous results demonstrating the existence of non-trivial gaps between the two lattice types. As previously mentioned, only one choice of outer springs in the triatomic-like mass-in-mass unit cell has quantized Zak's phase which enables us to investigate the topology of the band gaps. The other two cases are having non-quantized geometric phase. However, despite the triatomic-like lattices with unit cell springs $k_1 < k_2 = k_3$ and $k_1 > k_2 = k_3$ having quantized geometric phases with different topology, it is difficult to construct a large chain from these two lattice types since they exhibit different band structures due to the reasons given before. Therefore, in the next sub-section, it will be attempted to construct the finite lattices from the triatomic-like sub-lattices with the same band structure properties but not necessarily quantized geometric phases. In [59], the authors demonstrated the possibility of the existence of interface states in one-dimensional lattices with multi-degree of freedom unit cells and coexisting quantized and non-quantized geometric phases due to hidden inversion symmetry in a subspace of the system. Some authors also suggested the methodology for quantization of the geometric phase [58] while others proposed the corrected formula for Zak's phase of the one-dimensional (1D) lattice [60] when the unit cell lacks the centered inversion axis. However, such investigation is out of the scope of this study and the existence of interface states will be assessed through the investigation of the bulk and interface mode spectrum of finite lattices.

4.2. Dynamics of finite inerter-based lattices with local resonators and interface

Here, we first study the dynamics of finite one-dimensional undamped ($c_a = c_b = 0$) inerter-based lattices with local resonators to demonstrate the existence of band gaps and corresponding interface modes. The chain is constituted of two sub-lattices connected at the interface (see Figure 2). First, we investigate the eigenvalue spectrum corresponding to a variation of two different sub-lattice springs connecting outer masses from $\gamma = -1$ to $\gamma = 1$ such that the sum of $k_1 = k(1+\gamma)$ and $k_2 = k(1-\gamma)$ is equal to the double value of the mean stiffness $k_1 + k_2 = 2k$. However, in the case of triatomic-like lattices the summation of springs in combination $k_1 = k(1+\gamma)$, $k_2 = k_1$ and $k_3 = k(1-\gamma)$ or $k_1 = k(1+\gamma)$, $k_2 = k(1-\gamma)$ and $k_3 = k_1$, is not constant for variations of γ (odd number of outer springs). The case $\gamma = 0$ corresponds to the band-folding diagrams in the previous dispersion analysis of lattice unit cells when all outer springs have equal stiffness. Moreover, the frequency response functions (FRF) of the interface mass are given to show the effect of inerters and changes in the locally resonant mass on modes localized at the interface between the two sub-lattices. In all the presented cases in this sub-section, we adopted $N = 30$ unit cells on each side of the interface.

Figure 5 shows bulk and interface spectra of the fixed-free and free-free inerter-based diatomic-chains with local resonators (configuration from Figure 2b) when $j_a = j_b = 0.02$. In both cases, one can identify three band gaps (apart from the zero-frequency gap), where two gaps are closing at $\gamma = 0$ and the middle gap remains open. Figure 5a shows eigenvalue spectra and corresponding highlighted eigenmodes of the fixed-free chain demonstrating the existence of four characteristic interface modes for $\gamma > 0$. However,

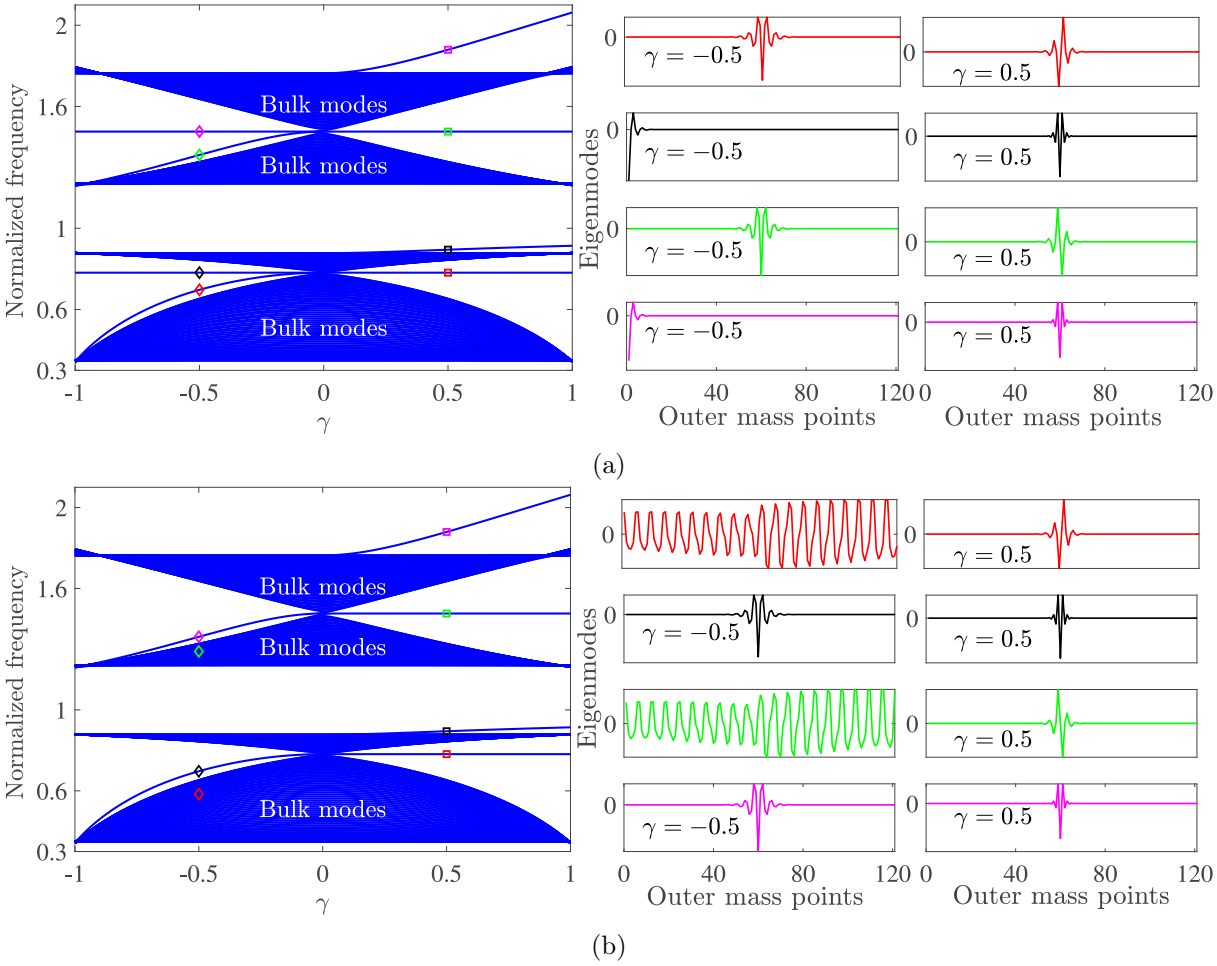

Fig. 5: The eigenvalue spectrum and highlighted eigenmodes of the finite inerter-based diatomic-like mass-in-mass chains with $N = 30$ unit cells on each side of the interface, $j_a = j_b = 0.02$, varying stiffness parameter γ and (a) fixed-free edge conditions (b) free-free edge conditions

previous topological analysis demonstrates that only gaps I and III are non-trivial, which indicates the existence of non-trivial interface states. According to the observations in [61] for simple diatomic-like mass-spring chains, those modes where interface mass is at rest $u^0_{(1)a} = 0$ while neighboring masses are of equal amplitude but opposite sign $u^0_{(2)a} = -u^{-1}_{(2)a}$ can be defined as symmetric modes. In the case of anti-symmetric mode shapes, the interface mass and the neighboring masses are having some displacement amplitudes such that $u^0_{(1)a} \neq 0$ and $u^0_{(2)a} = u^{-1}_{(2)a}$. A similar observation is also valid for triatomic-like mass-spring chains. Following this, it can be noticed that the interface modes emerging within gaps I and III in Figure 5a are symmetric about the interface mass for $\gamma > 0$. Therefore, natural frequencies of such interface modes remain constant for variations of γ when there are two adjacent heavy springs at the interface. On the other hand, the interface modes that appear within gap II are trivial and will migrate into the bulk for changes in the interface springs $\gamma < 0$ i.e. for the weak stiffness interface springs. Therefore, only two interface modes exist on the left side ($\gamma < 0$) of the spectra having antisymmetric mode shapes about the interface mass and whose frequency varies with the change of stiffness in the interface springs. However, two edge modes of constant frequency also exist on the left side of the spectra ($\gamma < 0$), which are localized at the fixed edge of the lattice. These two modes will disappear in the free-free chain whose spectrum is given in Figure 5b. The other two interface modes will remain the same in the configuration with free boundaries.

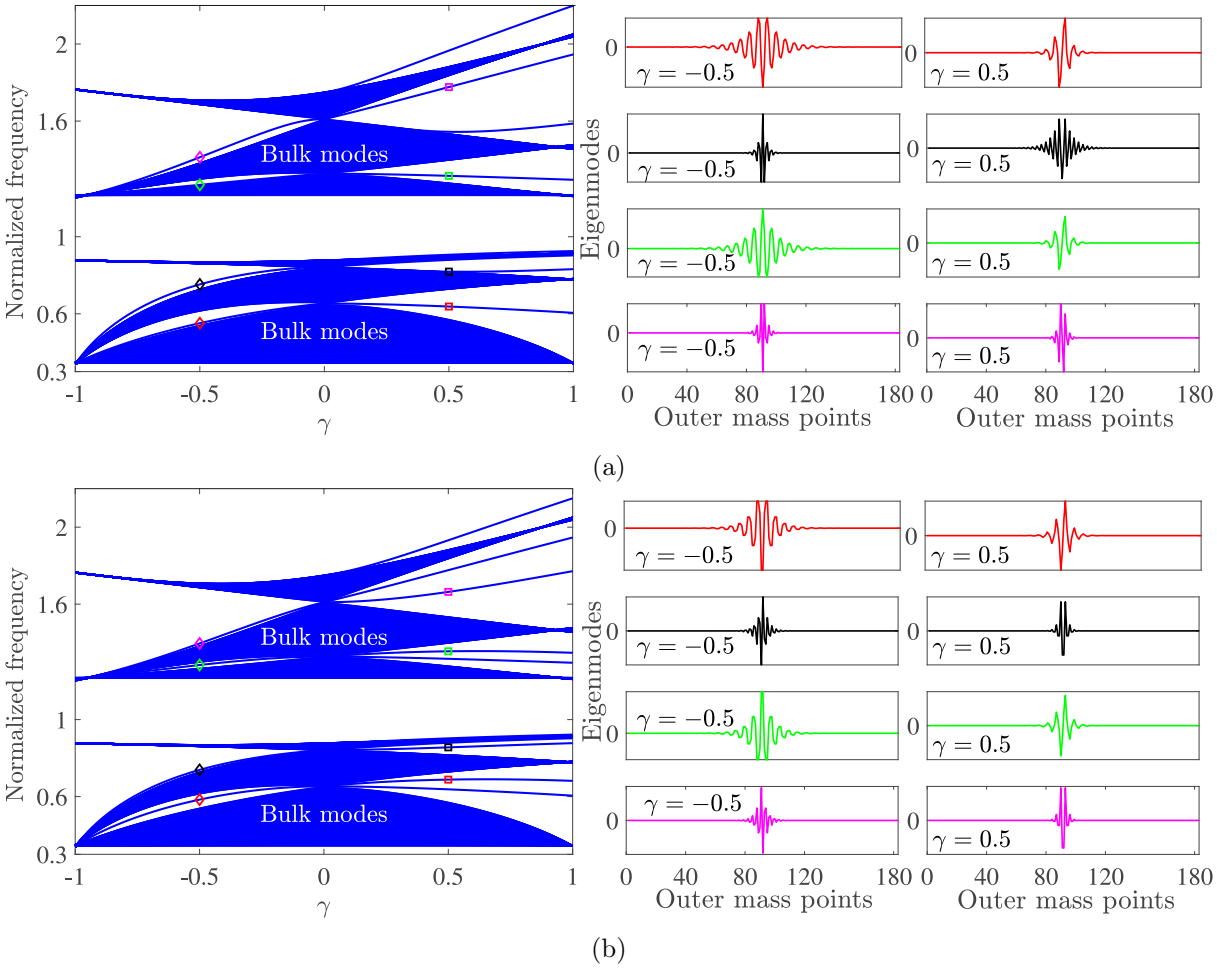

Fig. 6: The eigenvalue spectrum and highlighted eigenmodes of the finite fixed-free inerter-based triatomic-like mass-in-mass chains with $N = 30$ unit cells on each side of the interface, $j_a = j_b = 0.02$ and varying stiffness parameter γ: (a) configuration from Fig. 2c (b) configuration from Fig. 2d.

When the first outer mass on the left side of the chain is connected to the fixed edge through a stronger stiffness spring $k_2 = k(1 - \gamma)$, an edge state occurs for $\gamma < 0$ (weak stiffness springs at the interface) at the same frequency as the symmetric interface mode for $\gamma > 0$ (stronger stiffness springs at the interface). When a fixed boundary condition is imposed on the edge, that edge is behaving as a mass whose displacement is set to zero, therefore resembling the behavior of the symmetric interface mode. This observation is similar to the behavior of the semi-infinite one-dimensional chain studied in [9], where edge localized modes emerge in the configuration when a stronger stiffness spring is connected to the fixed edge. It should be also mentioned that the introduction of the fixed-fixed edge conditions in the chain would result in additional edge localized modes (especially in the triatomic-like mass-in-mass chains), therefore, this case of edge conditions is not elaborated in this study.

Next, we investigate the eigenvalue spectrum of the finite fixed-free inerter-based triatomic-like mass-in-mass chains with local resonators Figure 6. Here, in the configuration from Figure 2c one can observe five characteristic band gaps (excluding the zero-frequency gap) between the bulk modes that are crossed with corresponding interface modes that exist on both, left ($\gamma < 0$) and right ($\gamma > 0$) side of the spectrum Figure 6a. Four characteristic interface modes exist for $\gamma = -0.5$ and $\gamma = 0.5$, with

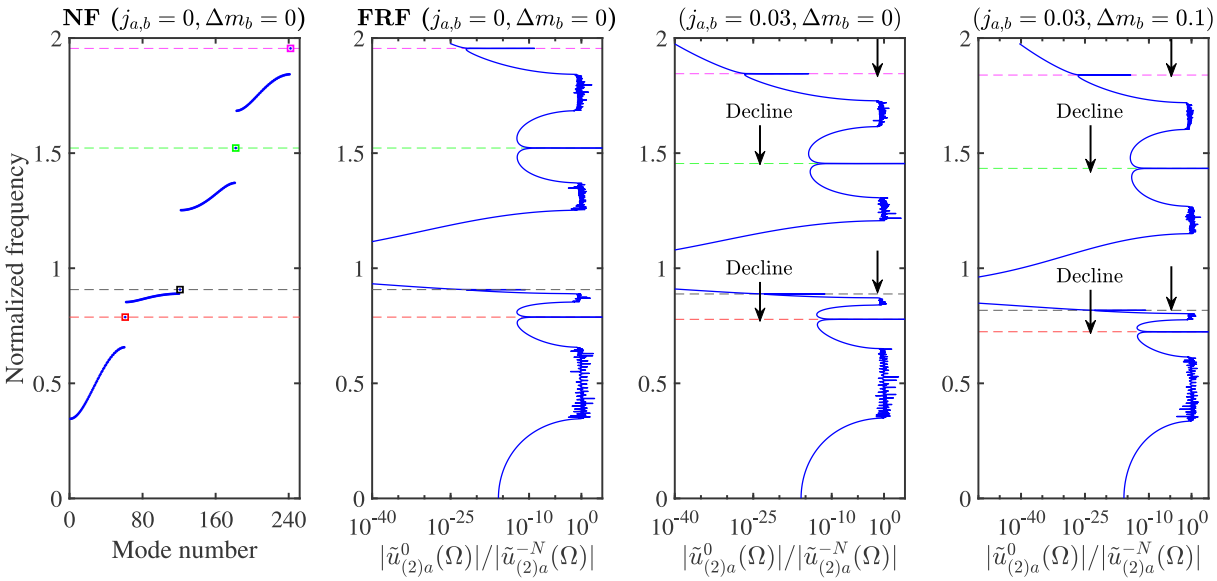

Fig. 7: Natural frequencies and frequency response function of the finite undamped diatomic-like mass-in-mass chain (configuration from Fig. 2b when $c_a = c_b = 0$) for $\gamma = 0.5$ and $N = 30$ unit cells on each side of the interface. The case with $j_a = j_b = 0$ and $\Delta m = 0$ refers to the initial configuration without inerters and changes in the locally resonant mass.

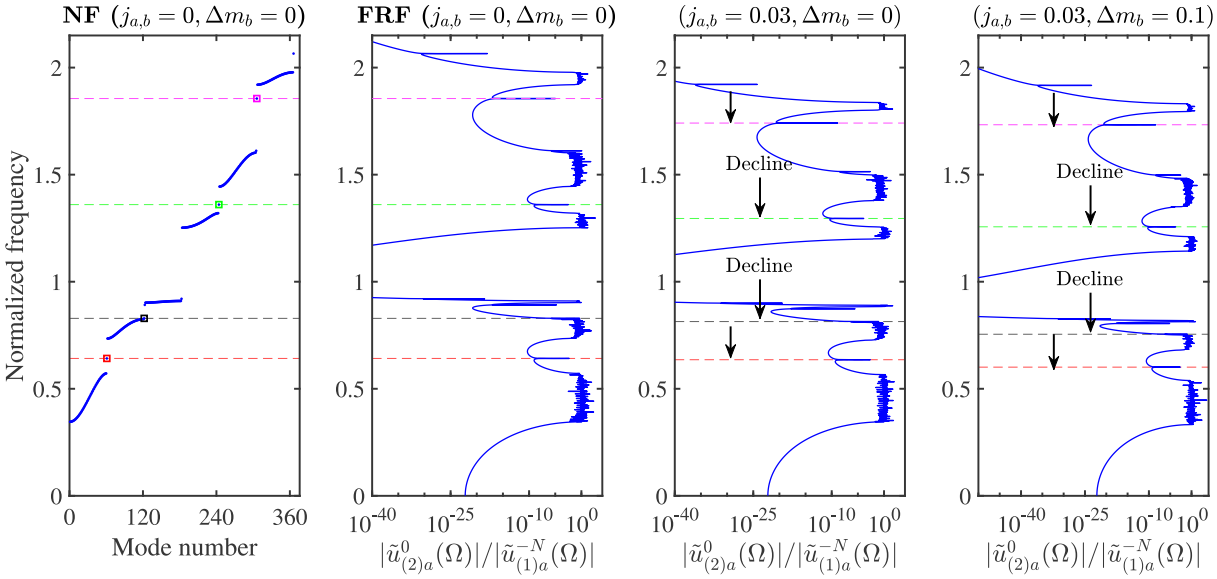

Fig. 8: Natural frequencies and frequency response function of the finite undamped triatomic-like mass-in-mass chain (configuration from Fig. 2c when $c_a = c_b = 0$) for $\gamma = 0.5$ and $N = 30$ unit cells on each side of the interface. The case with $j_a = j_b = 0$ and $\Delta m = 0$ refers to the initial configuration without inerters and changes in the locally resonant mass.

eigenmodes of highlighted eigenstates given in separate panels. These mode shapes show that three eigenmodes are symmetric about the interface mass while one of them is the anti-symmetric one. However, the behavior of the symmetric interface modes is different from those in the diatomic-like chains since their frequency varies with γ owing to the change in overall stiffness (odd number of outer springs). All four modes on the left side of the spectrum ($\gamma < 0$) display the antisymmetric modes shapes and the frequency of these modes also varies with γ. One can notice that two of the gaps on the left side of the spectrum are very narrow, which is attributed to the ratio of the stiffnesses of the

outer springs that are responsible for the band-folding induced gaps. Despite being very narrow, some interface modes also exist within these gaps.

Further, observation of the eigenvalue spectrum of the finite chain in the configuration from Figure 2d shows the same number of band gaps and interface modes on the left side of the spectrum ($\gamma < 0$) as in the previous case. Eigenmodes of the four highlighted interface mode eigenstates for $\gamma = -0.5$ and $\gamma = 0.5$ reveals their localization at the interface. Only two interface modes can be viewed as symmetric about the interface mass whose frequency varies with γ. The rest of the identified interface states are having antisymmetric mode shapes and their frequency also varies with the change in the stiffness of interface springs. Note that some additional modes, which can be seen within the same gaps on the right side of the spectrum, are edge modes localized at the fixed boundary of the chain. It is already discussed in dispersion and topological analysis that in some triatomic-like unit cells certain permutations of outer springs lack the unit cell symmetry, which would result in a non-quantized Zak's phase. However, in the literature, it was proven how some hidden symmetries and topologically protected interface modes can still exist in lattices with co-existing quantized and non-quantized Zak's phase. Moreover, similar spectrum analysis in [41] demonstrated that topologically protected interface modes can also exist in one-dimensional polyatomic chains, though they are not as flat as the one in the simple diatomic lattices. Even at the first sight some of the interface modes in triatomic-like mass-in-mass lattices behave similar to the trivial defect modes, there is a high possibility that they have a non-trivial nature. The proof of these interface mode properties would require additional investigation, which could be an interesting topic for future study.

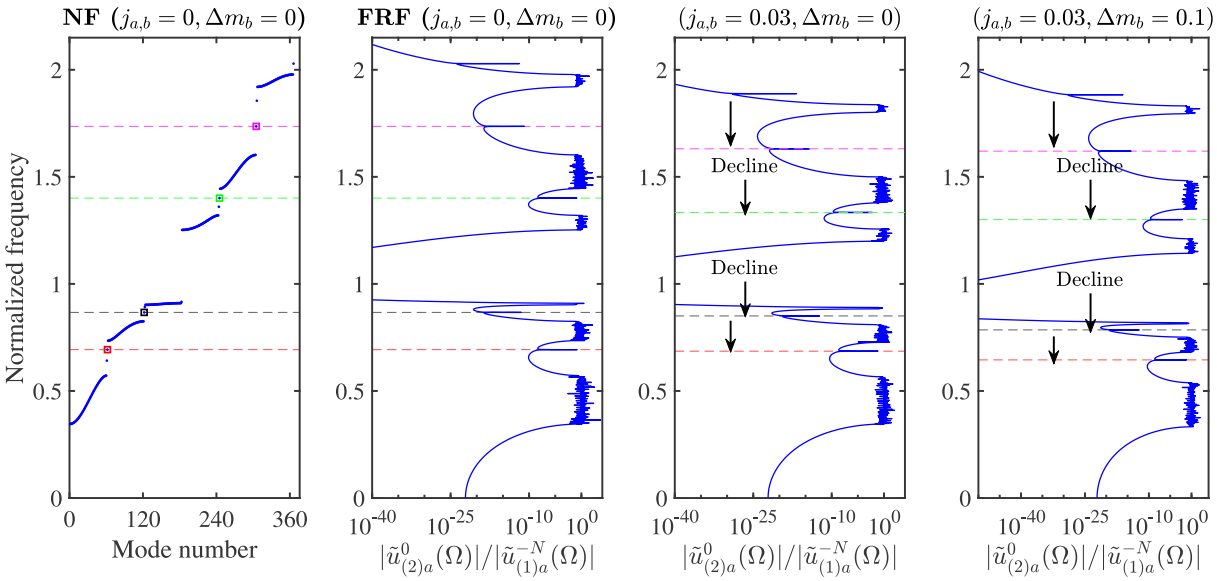

Fig. 9: Natural frequencies and frequency response function of the finite undamped triatomic-like mass-in-mass chain (configuration from Fig. 2d when $c_a = c_b = 0$) for $\gamma = 0.5$ and $N = 30$ unit cells on each side of the interface. The case with $j_a = j_b = 0$ and $\Delta m = 0$ refers to the initial configuration without inerters and changes in the locally resonant mass

Figure 7 shows natural frequencies (NFs) and frequency response function (FRF) of the finite fixed-free inerter-based diatomic-like mass-in-mass chain when stiffness of outer springs is defined by $\gamma = 0.5$ (configuration from Figure 2b). Here, NFs are given only for the lattice configuration without inerters to demonstrate the existence of interface mode frequencies, which are then validated through the FRF plots of the nearest neighbor mass to the interface mass (since the interface mass is at rest in symmetric mode shapes). The

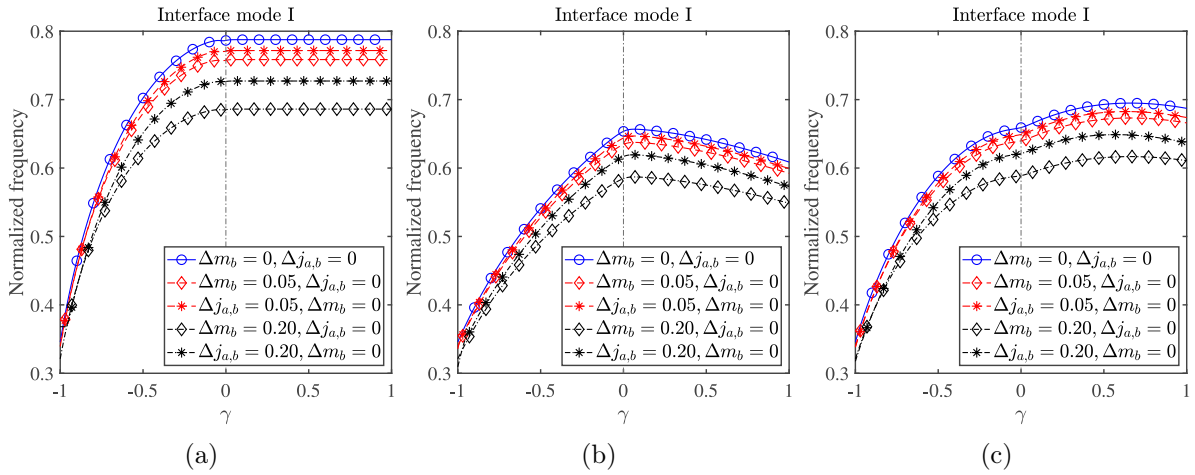

Fig. 10: The comparison of the effects of perturbations in locally resonant mass and inertance on the first interface mode frequency of the finite fixed-free diatomic-like and triatomic-like mass-in-mass chains in configurations from (a) Fig. 2b; (b) Fig. 2c; (b) Fig. 2d. The first interface mode frequency curves in the perturbed cases are compared against the initial configuration (blue solid line) where $\Delta m_b = m_b - m_{b(0)} = 0$ and $\Delta j_{a,b} = j_{a,b} - j_{a,b(0)} = 0$ for $m_{b(0)} = 0.5$ and $j_{a,b(0)} = 0$.

FRF results demonstrate the existence of several interface modes in the initial configuration without inerters $j_a = j_b = 0$ and changes in the locally resonant mass $\Delta m = 0$. Four characteristic interface mode frequencies are highlighted and their behavior is followed in different configurations. The next two FRF plots show how the introduction of inerters with low inertance $j_a = j_b = 0.03$ and $\Delta m = 0.1$ change in the locally resonant mass affect interface mode frequencies. If only inerters are introduced without changes in the locally resonant mass, a significant shifting of higher frequency interface modes to lower values occurs while this change in the lower frequency interface modes is minor. On the other hand, the combined effect of inerters and increase of locally resonant mass (for $\Delta m = 0.1$) significantly shifts both lower and higher frequency interface modes to lower values.

Figure 8 shows NF and FRF of the finite fixed-free triatomic-like mass-in-mass chains in configuration from Figure 2c (when $\gamma = 0.5$). NF of the chain in the initial configuration without inerters $j_a = j_b = 0$ and no changes in the locally resonant mass $\Delta m = 0$ shows several interface modes, where again we chose four characteristic modes within the band gaps I, II, IV, and V and follow their behavior in the case when inerters and changes in the locally resonant masses are introduced. The first FRF plot from the left side confirms the existence of interface modes that can be seen in the NFs plot. Introduction of inerters with inertance $j_a = j_b = 0.03$ and $\Delta m = 0$ displays significant shifting of the higher frequency interface modes (gaps IV and V) to lower values while that change is small for the lower frequency interface modes (gaps I and II). However, by increasing the locally resonant mass for $\Delta m = 0.1$ and using the same inertance we can observe a significant decrease in the frequency of interface modes in both lower and higher frequency band gaps. Similar behavior of interface modes can be observed in Figure 9 in FRF plots of triatomic-like mass-in-mass chain in configuration from Figure 2d when $\gamma = 0.5$. Here, the largest effect on interface modes is achieved by combining the influence of inerters and perturbations in the locally resonant mass. However, one can notice that some of the states that can be seen in the NF plots are missing in the FRF. These results are in line with the conclusions from the spectrum analysis where it was shown how some of the states are localized at the fixed boundary of the chain and not at the interface.

Finally, to reveal the impact of inerters on the lowest frequency interface modes we

have chosen to show the first highlighted interface states of the fixed-free diatomic-like and triatomic-like mass-in-mass chains from Figure 5a and Figure 6 and observe their frequencies for variations of the stiffness parameter γ as given in Figure 10. Here, the effects of perturbations in the locally resonant mass and inertance on the first interface mode frequency are compared. Same as previously, the perturbation in the locally resonant mass is defined as $\Delta m_b = m_b - m_{b(0)}$ and for the inertance as $\Delta j_{a,b} = j_{a,b} - j_{a,b(0)}$, with m_b and $j_{a,b}$ denoting the current perturbed parameters while $m_{b(0)} = 0.5$ and $j_{a,b(0)} = 0$ are values of the locally resonant mass and inertance, respectively, in the initial configuration. Figure 10a shows changes in the first interface mode frequency of the diatomic-like mass-in-mass chain. As discussed above, the first interface mode frequency varies for negative γ while it is a constant value for positive γ owing to the weak and strong stiffness interface springs, respectively. By introducing the inerters and increasing the value of inertia amplification parameters j_a and j_b (an increase of $\Delta j_{a,b}$), the frequency of the interface mode is shifted to lower values without significantly changing the shape of the interface mode frequency curve for varying γ. However, the same amount of perturbation in the locally resonant mass parameter shifts the first interface mode frequency to lower values more than the inertance. Therefore, inertance as a tuning parameter in mechanical lattices can have a different role than the locally resonant mass due to its larger effect on higher frequency interface modes and much weaker effect on lower frequency modes. Similar behavior can be observed for the finite chains with triatomic-like mass-in-mass unit cells given in Figure 10b and Figure 10c. Here, a larger effect on the first interface mode frequency for perturbations in the locally resonant mass can be also observed. Though shifting of the interface mode frequency becomes more pronounced for higher values of inertance, high values of inertia amplification could be difficult to achieve in some application scenarios due to limitations in design parameters of different types of inerter devices. Therefore, if only the first interface mode is the targeted mode to be tuned to lower frequency values, then the effects of perturbations in locally resonant mass should be used to achieve desired topological behavior of the periodic lattice systems.

4.3. Steady-state responses of damped inerter-based lattices with local resonators

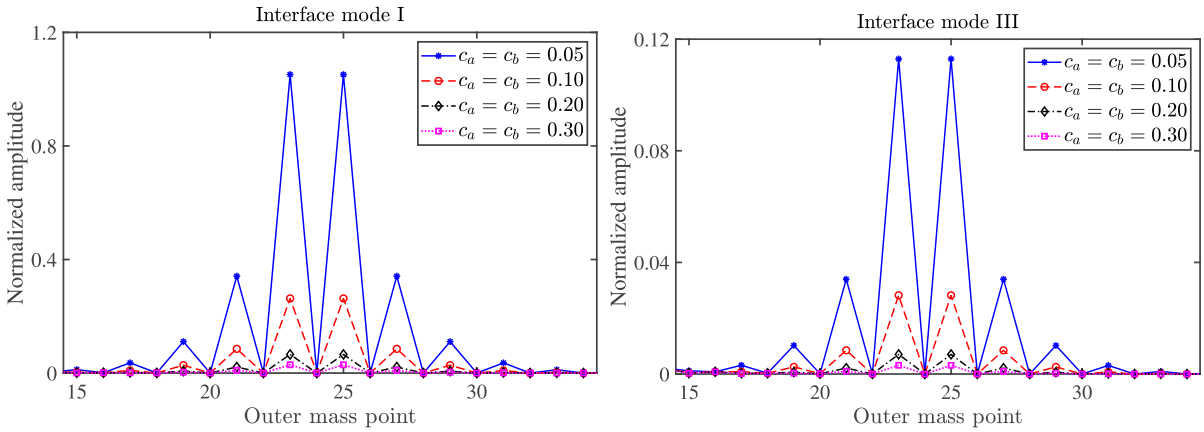

Fig. 11: Displacement amplitudes of the outer mass points of fixed-free inerter-based diatomic-like mass-in-mass chain in the configuration from Fig. 2b with $N = 12$ unit cells on each side of the interface and values of parameters $j_a = j_b = 0.02$ and $\gamma = 0.5$: (a) Interface mode I (b) Interface mode III.

In this part of the numerical study we are exploring the effect of arbitrary viscous

damping on normalized steady-state amplitudes of lattice points when the first mass in the lattice from the fixed side is excited with the frequency of particular interface modes. The amplitudes are obtained based on Eqs. 19-23 and the proposed solution given in Appendix A. We chose two characteristic modes located within the gaps that were characterized as non-trivial in the dispersion and topological analysis of unit cells of corresponding infinite lattices. Note that only the absolute values of the amplitudes are considered, which are then normalized with the amplitude of the excited mass. The frequencies of interface modes are adopted for $\gamma = 0.5$ and $j_a = j_b = 0.02$ and numerated according to the gap number in which they are situated, which can be also viewed in the corresponding spectrum plots in the previous sub-section. Figure 11 shows steady-state amplitudes of the finite diatomic-like mass-in-mass chain for different values of damping parameters $c_a = c_b$ and $N = 12$ unit cells on each side of the interface. The obtained results for interface mode I (Figure 11a) shows a significant effect of the viscous damping parameter on the existing interface mode amplitudes. Since the first interface mode is characterized as symmetric, only the neighboring masses are symmetrically displaced with respect to the interface mass while amplitudes far from the interface are at rest. The largest interface amplitudes are obtained for the case of small damping parameters $c_a = c_b = 0.05$ whose maximum value is greater than one i.e. the amplitude is larger than the amplitude of the exciting mass. An increase of damping significantly reduces the interface amplitudes that are almost completely attenuated for the larger values of damping parameters. A closer look at the interface mode III (Figure 11b) shows much lesser amplitudes with respect to the excitation amplitude for all damping cases. Again, one can observe that the largest interface amplitudes are obtained for the smallest damping parameter $c_a = c_b = 0.05$ while a significant reduction is achieved for larger damping parameters. Note that an increase in the number of unit cells in the lattice will lead to a cumulative effect of viscous damping elements in the chain and the interface mode amplitudes will be completely attenuated for large enough chains. A similar influence of damping on interface mode amplitudes was observed in [44].

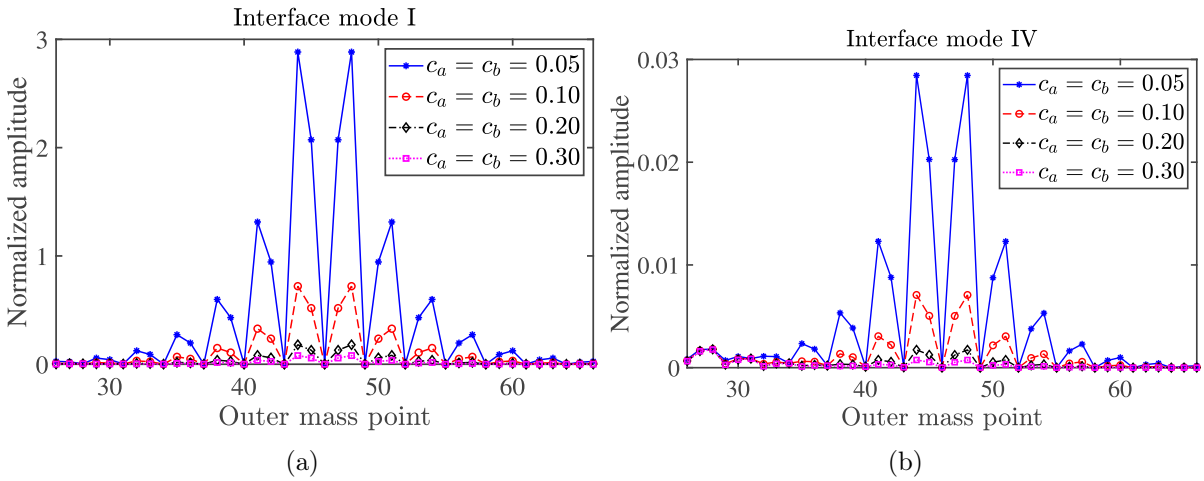

Fig. 12: Displacement amplitudes of the outer mass points of fixed-free inerter-based triatomic-like mass-in-mass chain in the configuration from Fig. 2c with $N = 15$ unit cells on each side of the interface and values of parameters $j_a = j_b = 0.02$ and $\gamma = 0.5$: (a) Interface mode I (b) Interface mode IV.

Similar observations can be made for the interface states of the finite inerter-based triatomic mass-in mass chains with damping and $N = 15$ unit cells on each side of the interface. Figure 12 shows interface mode amplitudes of the chain in configuration from

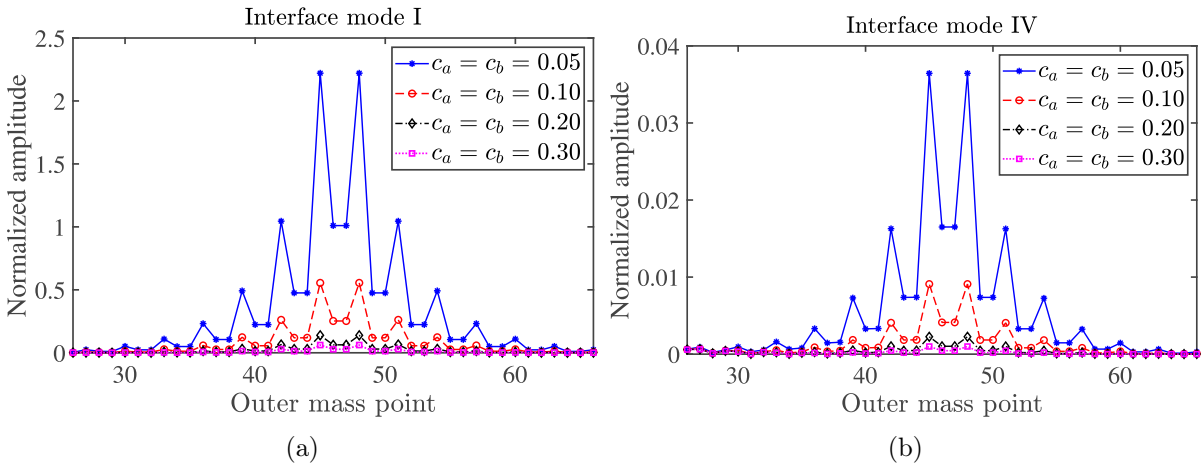

Fig. 13: Displacement amplitudes of the outer mass points of fixed-free inerter-based triatomic-like mass-in-mass chain in the configuration from Fig. 2d with $N = 15$ unit cells on each side of the interface and values of parameters $j_a = j_b = 0.02$ and $\gamma = 0.5$: (a) Interface mode I (b) Interface mode IV.

Figure 2c when $\gamma = 0.5$ and $j_a = j_b = 0.02$. The amplitude of the interface mode I exceed the magnitude of the excitation amplitude (three times) for the case of small damping $c_a = c_b = 0.05$ while the amplitudes of mass points far from the interface are at rest (Figure 12a). However, the interface amplitudes are largely attenuated for an increase in the value of damping parameters. Here, the interface mode is considered to be symmetric about the interface mass. Further, Figure 12b shows the lattice point amplitudes of the interface mode IV (situated in the fourth band gap e.g. see Figure 6a for details) that are much smaller than the amplitude of the exciting outer mass (around thirty times). Here, the interface mode amplitudes are the highest for the lowest value of damping $c_a = c_b = 0.05$ while they are almost completely attenuated for the damping parameter value $c_a = c_b = 0.3$. A similar effect of damping can be observed in Figure 13 for the triatomic-like mass-in-mass lattice configuration from Figure 2d, where a significant attenuation of interface mode amplitudes occurs for an increase of damping parameters. Here, the main difference can be noticed in the shape of interface mode amplitudes since there are no interface mass points at rest. This behavior of the interface mode amplitudes is the most similar to the behavior of anti-symmetric interface modes that was observed earlier in the literature [62].

It is well known that the damping effect is present in real engineering structures and systems and cannot be easily neglected if we want to accurately predict their dynamic behavior. This physical consequence is also important for large periodic chains, where different damping sources can exist in the lattice, especially when inerter elements are embedded into the lattice. Therefore, consideration of damping might be crucial for the reliable investigation of the existence of interface modes in mechanical metamaterials and periodic structures.

5. Conclusion

While topological insulators constitute a topic of significant current interest in condensed matter physics, an engineering route hitherto is less explored. One-dimensional locally acoustic chains to study exotic interface resonances serve as an intriguing platform to embark in this direction, which should be attested to the ubiquitous use of spring-mass models, both with and without inerters. This study illustrates the occurrence of interface

states in one-dimensional locally resonant acoustic chains with inerter elements. Dispersion and topological properties of two types of inerter-based unit cells having diatomic-like and triatomic-like mass-in-mass configurations were examined based on the Bloch wave dispersion and eigenvector topology analysis. The eigenvalue spectrum and frequency response functions of finite chains given as a block of two connected sub-lattices were studied to demonstrate the existence of interface states and the impact of inerters, changes in locally resonant masses, and damping on them. The main contributions of this work are:

- Based on dispersion and topological analysis of diatomic and triatomic mass-in-mass unit cells, we demonstrated that frequencies of individual bands could be shifted to lower values when introducing the inerters while keeping the topological properties of the original unit cell configuration without inerters. Moreover, the potential of band gaps for the existence of topologically protected edge/interface states is examined based on signs of band gaps.

- Dynamic analysis of finite inerter-based diatomic- and triatomic-like mass-in-mass chains confirms the existence of interface modes and their localization within both lower and higher frequency band gaps. Finally, it is demonstrated how an increase in inertia amplification parameters shifts the frequency of interface modes to lower values in a different manner than an increase of the locally resonant mass. It was shown that the best tunability of interface modes can be achieved by combining the effects of inertance and locally resonant mass.

- Investigation of the steady-state responses of outer mass lattice points demonstrated a significant influence of the arbitrary viscous damping on interface mode amplitudes, where complete attenuation of the amplitudes was observed for higher values of damping parameter. The attenuation effect was shown to be much more pronounced in higher frequency modes and for longer chains.

In this work, we revealed how inerter elements are capable of tuning edge/interface modes in one-dimensional locally resonant acoustic systems with more complex internal unit cell architecture. By introducing the inerters, we were able to keep the topological properties of original unit cell configurations and, at the same time, shift the frequency of interface modes. This property can be promising for consideration of inerters in passive control of topological properties of equivalent continuum elastic locally resonant acoustic systems. Moreover, we have shown how consideration of damping should be an unavoidable step when studying the edge/interface modes in real mechanical metamaterials. Conclusively, our work should have provided a tutorial, yet detailed study into contemporary topological mechanical configurations comprising novel vibrational localisations and their characterization. To this end, we believe that our findings should stimulate further interest along this line.

Acknowledgements

MC and SA acknowledges funding from European Union's Horizon 2020 research and innovation programme under the Marie Skłodowska-Curie grant agreement No. 896942 (METASINK). DK acknowledges the support by the Serbian Ministry of Education, Science and Technological Development through Mathematical Institute of the Serbian Academy of Sciences and Arts. JC acknowledges the support from the European Research Council (ERC) through the Starting Grant No. 714577 PHONOMETA and from the MINECO through a Ramón y Cajal grant (Grant No. RYC-2015-17156). JC also

acknowledges the support from the Comunidad de Madrid (Spain) - multiannual agreement with UC3M ("Excelencia para el Profesorado Universitario" - EPUC3M14) - Fifth regional research plan 2016-2020.

Appendix A. The solution for the system with arbitrary viscous damping

A solution to the equations of motion Eq. 23 of finite diatomic-like or triatomic-like chains with arbitrary viscous damping can be found in the state space (e.g. see [63]). If the overall system has m-degrees of freedom, the state form of the motion equations is given as

$$\dot{\mathbf{x}}(t) = \mathbf{A}\mathbf{x}(t) + \mathbf{B}\mathbf{f}(t) \tag{A.1}$$

where

$$\mathbf{A} = \begin{bmatrix} \mathbf{0} & \mathbf{I} \\ -\mathbf{M}^{-1}\mathbf{K} & -\mathbf{M}^{-1}\mathbf{C} \end{bmatrix}, \mathbf{B} = \begin{bmatrix} \mathbf{0} \\ -\mathbf{M}^{-1} \end{bmatrix}$$

and $\mathbf{x} = \left[\mathbf{q}^T, \dot{\mathbf{q}}^T\right]$ is the $2m$-dimensional state vector. The given matrix $\mathbf{A}$ is the non-symmetric matrix for which $\mathbf{A}^T \neq \mathbf{A}$. The further procedure will require to find right $\mathbf{x}_i$, $i = 1, 2, ..., 2m$ and left $\mathbf{y}_i$ eigenvectors of $\mathbf{A}$ by solving the corresponding eigenvalue problems for $\mathbf{A}$ and $\mathbf{A}^T$ when $\mathbf{f} = 0$. If $\mathbf{X} = [\mathbf{x}_1, \mathbf{x}_2, ...\mathbf{x}_{2m}]$ is the matrix of right and $\mathbf{Y} = [\mathbf{y}_1, \mathbf{y}_2, ...\mathbf{y}_{2m}]$ is the matrix of left eigenvectors and $\mathbf{\Lambda} = [\lambda_1, \lambda_2, ..., \lambda_{2m}]$ is the matrix of eigenvalues, then the following relations should hold

$$\mathbf{Y}^T\mathbf{X} = \mathbf{I}, \quad \mathbf{Y}^T\mathbf{A}\mathbf{X} = \mathbf{\Lambda}, \quad \mathbf{Y}^T = \mathbf{X}^{-1}. \tag{A.2}$$

By considering the excitation as $\mathbf{f}(t) = \mathbf{f}_0 \exp(\mathrm{i}\Omega t)$, where $\mathbf{f}_0$ is the vector of force amplitudes, we can obtain the final solution for the state vector as

$$\mathbf{x}(t) = \sum_{v=1}^{2m} \frac{\mathbf{y}_v^T \mathbf{B}\mathbf{f}_0}{\mathrm{i}\Omega - \lambda_v} \mathbf{x}_v \exp(\mathrm{i}\Omega t). \tag{A.3}$$

Note that only real part of the response should be retained if the excitation is $\mathbf{f}(t) = \mathbf{f}_0 \cos(\mathrm{i}\Omega t)$ and imaginary part if $\mathbf{f}(t) = \mathbf{f}_0 \sin(\mathrm{i}\Omega t)$.

References

[1] X.-L. Qi, S.-C. Zhang, Topological insulators and superconductors, Rev. Mod. Phys. 83 (2011) 1057. https://doi.org/10.1103/RevModPhys.83.1057

[2] F. Zangeneh-Nejad, A. Alù, R. Fleury, Topological wave insulators: a review, C. R. Phys. 21 (2020) 467–499. https://doi.org/10.5802/crphys.3

[3] B. Yang, H. Zhang, T. Wu, R. Dong, X. Yan, X. Zhang, Topological states in amorphous magnetic photonic lattices, Phys. Rev. B 99 (2019) 045307. https://doi.org/10.1103/PhysRevB.99.045307

[4] J. Chen, H. Huang, S. Huo, Z. Tan, X. Xie, J. Cheng, G.-l. Huang, Self-ordering induces multiple topological transitions for in-plane bulk waves in solid phononic crystals, Phys. Rev. B 98 (2018) 014302. https://doi.org/10.1103/PhysRevB.98.014302

[5] X. Zhang, M. Xiao, Y. Cheng, M.-H. Lu, J. Christensen, Topological sound, Commun. Phys. 1 (1) (2018) 1–13. https://doi.org/10.1038/s42005-018-0094-4

[6] S. D. Huber, Topological mechanics, Nat. Phys. 12 (2016) 621–623. https://doi.org/10.1038/nphys3801

[7] P. Deymier, K. Runge, One-dimensional mass-spring chains supporting elastic waves with non-conventional topology, Crystals 6 (2016) 44. https://doi.org/10.3390/cryst6040044

[8] J. Attig, K. Roychowdhury, M. J. Lawler, S. Trebst, Topological mechanics from supersymmetry, Phys. Rev. Res. 1 (2019) 032047. https://doi.org/10.1103/PhysRevResearch.1.032047

[9] H. Chen, H. Nassar, G. Huang, A study of topological effects in 1d and 2d mechanical lattices, J. Mech. Phys. Solids 117 (2018) 22–36. https://doi.org/10.1016/j.jmps.2018.04.013
[10] D. Pan, R. Yu, H. Xu, F. J. G. de Abajo, Topologically protected dirac plasmons in a graphene superlattice, Nat. Commun. 8 (2017) 1–7.
[11] B. Bahari, A. Ndao, F. Vallini, A. El Amili, Y. Fainman, B. Kanté, Nonreciprocal lasing in topological cavities of arbitrary geometries, Science 358 (2017) 636–640. https://www.science.org/doi/10.1126/science.aao4551
[12] Y. Liu, X. Chen, Y. Xu, Topological phononics: from fundamental models to real materials, Adv. Funct. Mater. 30 (2020) 1904784. https://doi.org/10.1002/adfm.201904784
[13] S. H. Mousavi, A. B. Khanikaev, Z. Wang, Topologically protected elastic waves in phononic metamaterials, Nat. Commun. 6 (2015) 1–7. https://doi.org/10.1038/ncomms9682
[14] B.-Z. Xia, S.-J. Zheng, T.-T. Liu, J.-R. Jiao, N. Chen, H.-Q. Dai, D.-J. Yu, J. Liu, Observation of valleylike edge states of sound at a momentum away from the high-symmetry points, Phys. Rev. B 97 (2018) 155124. https://doi.org/10.1103/PhysRevB.97.155124
[15] H. Fan, B. Xia, L. Tong, S. Zheng, D. Yu, Elastic higher-order topological insulator with topologically protected corner states, Physical Rev. Lett. 122 (2019) 204301. https://doi.org/10.1103/PhysRevLett.122.204301
[16] Z. Zhang, Y. Gu, H. Long, Y. Cheng, X. Liu, J. Christensen, Subwavelength acoustic valley-hall topological insulators using soda cans honeycomb lattices, Research 2019. https://doi.org/10.34133/2019/5385763
[17] Muhammad, W. Zhou, C. Lim, Topological edge modeling and localization of protected interface modes in 1d phononic crystals for longitudinal and bending elastic waves, Int. J. Mech. Sci. 159 (2019) 359–372. https://doi.org/10.1016/j.ijmecsci.2019.05.020
[18] Y. Ruan, X. Liang, X. Hua, C. Zhang, H. Xia, C. Li, Isolating low-frequency vibration from power systems on a ship using spiral phononic crystals, Ocean Eng. 225 (2021) 108804. https://doi.org/10.1016/j.oceaneng.2021.108804
[19] M. Xiao, G. Ma, Z. Yang, P. Sheng, Z. Zhang, C. T. Chan, Geometric phase and band inversion in periodic acoustic systems, Nat. Phys. 11 (2015) 240–244. https://doi.org/10.1038/nphys3228
[20] Y. Liu, L. Jin, H. Wang, D. Liu, Y. Liang, Topological interface states in translational metamaterials for sub-wavelength in-plane waves, Int. J. Mech. Sci. 197 (2021) 106308. https://doi.org/10.1016/j.ijmecsci.2021.106308
[21] Y. Xia, A. Erturk, M. Ruzzene, Topological edge states in quasiperiodic locally resonant metastructures, Phys. Rev. Appl. 13 (2020) 014023. https://doi.org/10.1103/PhysRevApplied.13.014023
[22] D. J. Apigo, K. Qian, C. Prodan, E. Prodan, Topological edge modes by smart patterning, Phys. Rev. Mater. 2 (2018) 124203. https://doi.org/10.1103/PhysRevMaterials.2.124203
[23] X. Ni, K. Chen, M. Weiner, D. J. Apigo, C. Prodan, A. Alu, E. Prodan, A. B. Khanikaev, Observation of hofstadter butterfly and topological edge states in reconfigurable quasi-periodic acoustic crystals, Commun. Phys. 2 (2019) 1–7. https://doi.org/10.1038/s42005-019-0151-7
[24] L. Fan, Y. He, X. Zhao, X.-a. Chen, Subwavelength and broadband tunable topological interface state for flexural wave in one-dimensional locally resonant phononic crystal, J. App. Phys. 127 (2020) 235106. https://doi.org/10.1063/5.0001548
[25] H. Wang, D. Liu, W. Fang, S. Lin, Y. Liu, Y. Liang, Tunable topological interface states in one-dimensional extended granular crystals, Int. J. Mech. Sci. 176 (2020) 105549. https://doi.org/10.1016/j.ijmecsci.2020.105549
[26] W. M. Kuhnert, P. J. P. Gonçalves, D. F. Ledezma-Ramirez, M. J. Brennan, Inerter-like devices used for vibration isolation: a historical perspective, J. Franklin Inst. https://doi.org/10.1016/j.jfranklin.2020.11.007
[27] M. C. Smith, The inerter: a retrospective, Annu. Rev. Control Robot. Auton. Syst. 3 (2020) 361–391. https://doi.org/10.1146/annurev-control-053018-023917
[28] S. Krenk, J. Høgsberg, Tuned resonant mass or inerter-based absorbers: unified calibration with quasi-dynamic flexibility and inertia correction, Proc. R. Soc. A 472 (2016) 20150718. https://doi.org/10.1098/rspa.2015.0718
[29] Z. Zhao, R. Zhang, C. Pan, Q. Chen, Y. Jiang, Input energy reduction principle of structures with generic tuned mass damper inerter, Struct. Health Monit. 28 (2021) e2644. https://doi.org/10.1002/stc.2644
[30] Y. Wen, Z. Chen, X. Hua, Design and evaluation of tuned inerter-based dampers for the seismic control of mdof structures, J. Struct. Eng. 143 (2017) 04016207. https://doi.org/10.1061/(ASCE)ST.1943-541X.0001680
[31] G. Alotta, G. Failla, Improved inerter-based vibration absorbers, Int. J. Mech. Sci. 192 (2021)

106087. https://doi.org/10.1016/j.ijmecsci.2020.106087
[32] S. Ying Zhang, Y.-Y. Li, J. Z. Jiang, S. A. Neild, J. H. Macdonald, A methodology for identifying optimum vibration absorbers with a reaction mass, Proc. R. Soc. A 475 (2019) 20190232. https://doi.org/10.1098/rspa.2019.0232
[33] P. P. Kulkarni, J. M. Manimala, Longitudinal elastic wave propagation characteristics of inertant acoustic metamaterials, J. App. Phys. 119 (2016) 245101. https://doi.org/10.1063/1.4954074
[34] H. Al Ba'ba'a, D. DePauw, T. Singh, M. Nouh, Dispersion transitions and pole-zero characteristics of finite inertially amplified acoustic metamaterials, J. App. Phys. 123 (2018) 105106. https://doi.org/10.1063/1.5019703
[35] F. Sun, L. Xiao, Bandgap characteristics and seismic applications of inerter-in-lattice metamaterials, J. Eng. Mech. 145 (2019) 04019067. https://doi.org/10.1061/(ASCE)EM.1943-7889.0001642
[36] M. Cajić, J. Christensen, S. Adhikari, Tuning of topological interface modes in an elastic beam array system with inerters, Int. J. Mech. Sci. (2021) 106573. https://doi.org/10.1016/j.ijmecsci.2021.106573
[37] F. Jamil, F. Chen, B. Deng, R. G. Parker, P. Wang, Inerter-based elastic metamaterials for band gap at extremely low frequency, Extreme Mech. Lett. 56 (2022) 101847. https://doi.org/10.1016/j.eml.2022.101877
[38] D. Zhao, M. Xiao, C. W. Ling, C. T. Chan, K. H. Fung, Topological interface modes in local resonant acoustic systems, Phys. Rev. B 98 (2018) 014110. https://doi.org/10.1103/PhysRevB.98.014110
[39] Z. Zhang, Y. Cheng, X. Liu, J. Christensen, Subwavelength multiple topological interface states in one-dimensional labyrinthine acoustic metamaterials, Phys. Rev. B 99 (2019) 224104. https://doi.org/10.1103/PhysRevB.99.224104
[40] Z. Chen, W. Zhou, C. Lim, Active control for acoustic wave propagation in nonlinear diatomic acoustic metamaterials, Int. J. Non-Linear Mech. 125 (2020) 103535. https://doi.org/10.1016/j.ijnonlinmec.2020.103535
[41] H. Al Ba'ba'a, M. Nouh, T. Singh, Dispersion and topological characteristics of permutative polyatomic phononic crystals, Proc. R. Soc. A 475 (2019) 20190022. https://doi.org/10.1098/rspa.2019.0022
[42] H. Al Ba'ba'a, X. Zhu, Q. Wang, Enabling novel dispersion and topological characteristics in mechanical lattices via stable negative inertial coupling, Proc. R. Soc. A 477 (2021) 20200820. https://doi.org/10.1098/rspa.2020.0820
[43] A. Aladwani, A. Mohammed, M. Nouh, Tunable dissipation in elastic metamaterials via methodic reconfiguration of inertant mechanical networks, Meccanica 57 (2022) 1337–1352. https://doi.org/10.1007/s11012-022-01482-z
[44] Z. Zheng, J. Yin, J. Wen, D. Yu, Multiple topological interface states in broadband locally resonant phononic crystals, J. App. Phys. 129 (2021) 184901. https://doi.org/10.1063/5.0043473
[45] S. Li, D. Zhao, H. Niu, X. Zhu, J. Zang, Observation of elastic topological states in soft materials, Nat. Commun. 9 (1) (2018) 1–9. https://doi.org/10.1038/s41467-018-03830-8
[46] Y. Liu, H. Wang, W. Fang, Q. Han, D. Liu, Y. Liang, Tunable control of subwavelength topological interface modes in locally resonance piezoelectric metamaterials, Compos. Struct. 276 (2021) 114541. https://doi.org/10.1016/j.compstruct.2021.114541
[47] M. C. Smith, Synthesis of mechanical networks: the inerter, IEEE Trans. Automat. Contr. 47 (2002) 1648–1662. https://doi.org/10.1109/TAC.2002.803532
[48] B. Van Damme, G. Hannema, L. Sales Souza, B. Weisse, D. Tallarico, A. Bergamini, Inherent non-linear damping in resonators with inertia amplification, App. Phys. Lett. 119 (2021) 061901. https://doi.org/10.1063/5.0061826
[49] S. Guo, Y. Liu, L. Xu, X. Guo, L. Zuo, Performance evaluation and parameter sensitivity of energy-harvesting shock absorbers on different vehicles, Veh. Syst. Dyn. 54 (2016) 918–942. https://doi.org/10.1080/00423114.2016.1174276
[50] Y. Mi, Z. Lu, X. Yu, Acoustic inerter: Ultra-low frequency sound attenuation in a duct, J. Acoust. Soc. Am. 148 (2020) EL27–EL32. https://doi.org/10.1121/10.0001476
[51] D. De Domenico, P. Deastra, G. Ricciardi, N. D. Sims, D. J. Wagg, Novel fluid inerter based tuned mass dampers for optimised structural control of base-isolated buildings, J. Franklin Inst. 356 (2019) 7626–7649. https://doi.org/10.1016/j.jfranklin.2018.11.012
[52] M. I. Hussein, I. Patrick, A. Banerjee, S. Adhikari, Metadamping in inertially amplified metamaterials: Trade-off between spatial attenuation and temporal attenuation, J. Sound Vib. 531 (2022) 116977. https://doi.org/10.1016/j.jsv.2022.116977
[53] A. Banerjee, S. Adhikari, M. I. Hussein, Inertial amplification band-gap generation by coupling a levered mass with a locally resonant mass, Int. J. Mech. Sci. 207 (2021) 106630. https://doi.org/

10.1016/j.ijmecsci.2021.106630
[54] C.-S. Lee, I.-F. Io, H.-c. Kao, Winding number and zak phase in multi-band ssh models, Chin. J. Phys. https://doi.org/10.1016/j.cjph.2022.05.007
[55] M. Xiao, Z. Zhang, C. T. Chan, Surface impedance and bulk band geometric phases in one-dimensional systems, Phys. Rev. X 4 (2014) 021017. https://doi.org/10.1103/PhysRevX.4.021017
[56] S. Li, J. Xu, X. Pu, T. Tao, H. Gao, X. Mei, Energy-harvesting variable/constant damping suspension system with motor based electromagnetic damper, Energy 189 (2019) 116199. https://doi.org/10.1016/j.energy.2019.116199
[57] X. An, H. Fan, C. Zhang, Wave dispersion in one-dimensional periodic graded metacomposites, J. Sound Vib. 409 (2017) 217–226. https://doi.org/10.1016/j.jsv.2017.08.002
[58] S. Sarkar, Quantization of geometric phase with integer and fractional topological characterization in a quantum ising chain with long-range interaction, Sci. Rep. 8 (2018) 1–20. https://doi.org/10.1038/s41598-018-24136-1
[59] Y.-X. Xiao, Z.-Q. Zhang, C. Chan, Coexistence of quantized and non-quantized geometric phases in quasi-one-dimensional systems without inversion symmetry, arXiv preprint arXiv:1605.00549. https://doi.org/10.1103/PhysRevLett.118.166803
[60] A. Marques, R. Dias, Generalization of zak's phase for lattice models with non-centered inversion symmetry axis, arXiv preprint arXiv:1707.06162. https://doi.org/10.48550/arXiv.1707.06162
[61] R. K. Pal, J. Vila, M. Leamy, M. Ruzzene, Amplitude-dependent topological edge states in nonlinear phononic lattices, Phys. Rev. E 97 (2018) 032209. https://doi.org/10.1103/PhysRevE.97.032209
[62] R. K. Pal, M. Ruzzene, Edge waves in plates with resonators: an elastic analogue of the quantum valley hall effect, New J. Phys. 19 (2017) 025001. https://doi.org/10.1088/1367-2630/aa56a2
[63] L. Meirovitch, Fundamentals of vibrations, Waveland Press, 2010.